CHAPTER 2

c0010

# Plasmas in Deposition Processes

**Scott G. Walton and J.E. Greene**


| | | | |
|---|---|---|---|
| p0010 | 2.1 | Introduction | 33 |
| p0015 | 2.2 | Particle Collisions, Energy, and Motion | 34 |
| p0020 | | 2.2.1 Collisions: Mean Free Path and Cross-Section | 34 |
| p0025 | | 2.2.2 Electron Kinetic Energy | 37 |
| p0030 | | 2.2.3 Electron Energy Distribution | 38 |
| p0035 | | 2.2.4 Collision Frequencies | 40 |
| p0040 | | 2.2.5 Reaction Rates | 42 |
| p0045 | | 2.2.6 Mobilities | 43 |
| p0050 | | 2.2.7 Conductivity and Diffusion | 44 |
| p0055 | | 2.2.8 Particle Motion in Magnetic Fields | 45 |
| p0060 | 2.3 | Plasma Parameters and Collective Behavior | 47 |
| p0065 | | 2.3.1 Plasma Sheaths | 48 |
| p0070 | | 2.3.2 Ambipolar Diffusion | 53 |
| p0075 | | 2.3.3 Plasma Oscillations | 54 |
| p0080 | 2.4 | Discharge Plasmas | 55 |
| p0085 | | 2.4.1 Introduction | 55 |
| p0090 | | 2.4.2 Plasma Production and Breakdown | 57 |
| p0095 | | 2.4.3 Cold Cathode Discharges | 60 |
| p0100 | | 2.4.4 Magnetron Discharges | 62 |
| p0105 | | 2.4.5 RF Discharges | 63 |
| p0110 | 2.5 | Gas-Phase Plasma Reactions | 66 |
| p0115 | | 2.5.1 Introduction | 66 |
| p0120 | | 2.5.2 Electron–Atom Interactions | 67 |
| p0125 | | 2.5.3 Electron–Molecule Interactions | 68 |
| p0130 | | 2.5.4 Metastable Species and Processes | 70 |
| p0135 | | 2.5.5 Applications of Volume Reactions | 71 |
| p0140 | 2.6 | Plasma–Surface Interactions | 73 |
| p0145 | | 2.6.1 Introduction | 73 |
| p0150 | | 2.6.2 Ion Bombardment | 73 |
| p0155 | | 2.6.3 Electron Bombardment | 80 |
| p0160 | | 2.6.4 Photon Interactions | 81 |
| p0165 | | 2.6.5 Summary of Surface Reactions | 82 |
| p0170 | 2.7 | An Example: Magnetron Discharge for Deposition | 83 |
| p0175 | 2.8 | Summary | 86 |


Copyright © 2010 Elsevier Inc. All rights reserved.



ISBN: 978-0-8155-2031-3; PII: B978-0-8155-2031-3.00002-8; Author:Martin; Document ID:00002; Chapter ID:c0010

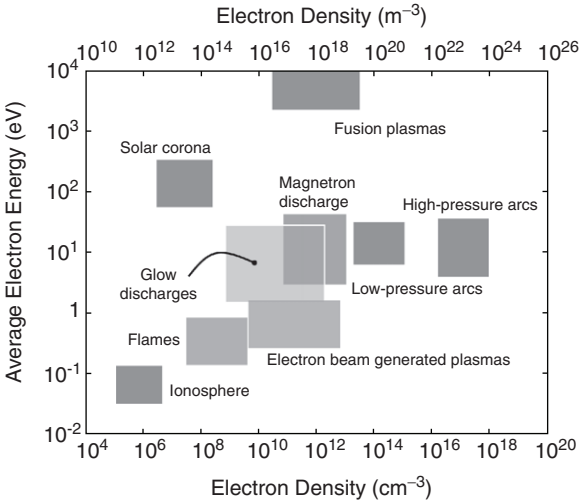


sp0010 **Figure 2.1: Ranges of average electron density and energy representative of various human-made and naturally occurring plasmas. (Adapted from [1].)**

## st0015 2.1 Introduction

p0185 Plasmas are partially ionized gases that contain approximately equal numbers of positively and negatively charged species. While plasmas are a common state of matter in the universe, they are rarely a natural occurrence on earth. Their unique properties, however, make them a powerful tool used in the modification of materials, ranging from material removal (etching) to the deposition of thin films and coatings. Plasmas are significantly different from 2.7 non-ionized gases; a consequence of the mass difference between the positively charged ions and negatively charged electrons as well as the energy of these species. Figure 2.1 shows the various types of plasmas, characterized by their electron densities and energies. Although a number of plasmas have been used in materials processing including arcs, flames, and electron beam-generated plasmas, the most common types are discharge plasmas, generated by applying an electric field to a volume of gas.

p0190 When an electric field is applied to an ionized gas, energy is transferred more rapidly to the electrons than to the ions. The transfer of kinetic energy from an electron to a heavy particle (atom, molecule, or ion) in an elastic collision is proportional to the mass ratio of electrons and heavy particles and therefore very small ($\sim 10^{-5}$). Consequently, at low pressures, where electron collisions are not as common, the electrons can accumulate sufficient kinetic energy to have a high probability of exciting, dissociating, or ionizing the heavier gas atoms and molecules during inelastic collisions. The production of these species, and their interactions with surfaces and growing films, is one of the reasons that low-pressure discharge plasmas

ISBN: 978-0-8155-2031-3; PII: B978-0-8155-2031-3.00002-8; Author:Martin; Document ID:00002; Chapter ID:c0010

have assumed a dominant role in materials processing. More specifically, the kinetic and potential energy delivered by both inert and reactive particles provide a means to change the physical and chemical properties of a material's surface. While these changes are initiated at the atomic or molecular scale, plasmas are routinely used to modify surface areas up to tens of square centimeters. In some cases, treatment areas are of the order of square meters. Examples of processing application areas that utilize plasmas, some covered in this book, include: sputter deposition, reactive sputter deposition, activated reactive evaporation, ion plating, plasma-assisted chemical vapor deposition (PACVD), plasma-assisted physical vapor deposition (PAPVD), plasma-assisted etching, and plasma polymerization.

p0195 This chapter should not be considered a comprehensive discussion of the extensive physics and chemistry of plasmas, but rather an introduction to plasmas; and so, we review fundamental characteristics of plasmas and discharge plasmas in particular, which are of importance in understanding the role of plasma processes in materials modification applications. With that in mind, we cover topics related to particle interactions, discharge physics, and plasma-surface interactions.

st0020 ## 2.2 Particle Collisions, Energy, and Motion

p0200 In any plasma-based materials processing application, the plasma parameters and resulting flux of species to the substrate determine the properties of the processed material or deposited film. Thus, it is important to understand the fundamental plasma properties and the gas-phase processes that influence these properties. The electron (or plasma) density, temperature, and energy distribution function are typically used to characterize the plasma. Collisions between electrons and heavy particles both sustain the plasma and determine the densities of reactive species while the collisions between the heavy particles further influence densities of reactive species, and particle fluxes at the substrate surfaces.

st0025 ### *2.2.1 Collisions: Mean Free Path and Cross-Section*

p0205 A plasma can be viewed as a medium in which energy is transported both in the gas and also to adjacent surfaces. In the case of a discharge plasma, electrical energy is transmitted, via an electric field, to a gas. The energetic gas particles are then used to promote chemical reactions in the gas or to interact with a surface to produce desirable effects such as surface reordering or sputtering. Thus, the process of energy exchange during collisions involving plasma-produced species is of fundamental importance.

p0210 Gas-phase collision probabilities are often expressed in terms of cross-sections. A related parameter is the mean free path or average distance traveled by particles between collisions. The mean free path $\lambda$ and collision cross-section $\sigma$ are generally defined by a simple relationship which treats the particles as hard or impenetrable spheres. The mean free path for

ISBN: 978-0-8155-2031-3; PII: B978-0-8155-2031-3.00002-8; Author:Martin; Document ID:00002; Chapter ID:c0010

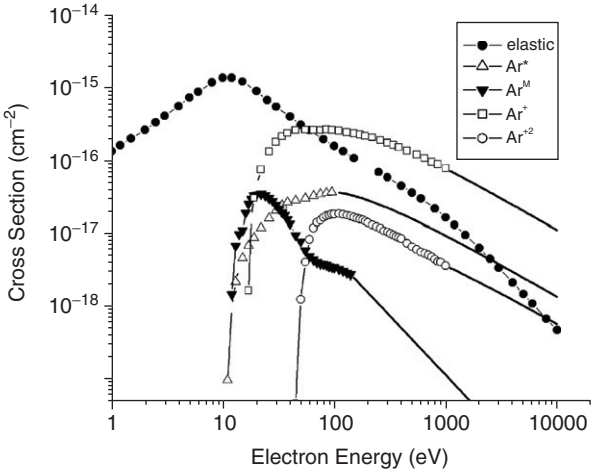


sp0015 **Figure 2.2: Collision cross-sections for electrons in argon. Products $Ar^+$ and $Ar^{+2}$ (from [2]), $Ar^m$ (from [3, 4]), and Ar* (from [4, 5]). Momentum transfer from [6].**

energetic particles passing through a gas of particle density $N$, where the gas particle is at rest is[1]

$$\lambda = 1/(N\sigma) \tag{2.1}$$

For electrons, the total collision cross-section can be written as

$$\sigma_{\text{tot}} = \sigma_{\text{elastic}} + \sigma_{\text{ex}} + \sigma_{\text{ion}} + \sigma_{\text{attach}} \tag{2.2}$$

where elastic, ex, ion, and attach subscripts indicate elastic, excitation, ionization, and attachment processes. In making plasmas calculations it is useful to note the common units and values found in the appendix. In this work, distances are expressed in centimeters (cm), energy in electron volts (eV), and pressure in torr. Figure 2.2 shows the cross-sections for electrons interacting with argon gas. The cross-sections are typically a strong function of the energy of the colliding species. For the case of electrons colliding with room temperature gas particles (atoms or molecules), the kinetic energy of the gas particles is generally much less than that of the electrons and can be neglected (the energy of gas particles at 300 K is approximately 0.039 eV). Consequently, only the electron energy is used in Figure 2.2. The figure shows that at low electron energies (below the ionization energy of 15.75 eV), the

[1] When the projectile and the target molecule have the same velocity, the case of thermal ions drifting through a gas for example, the mean free path is properly defined as $l = 1/\sqrt{2}Ns$.

ISBN: 978-0-8155-2031-3; PII: B978-0-8155-2031-3.00002-8; Author:Martin; Document ID:00002; Chapter ID:c0010

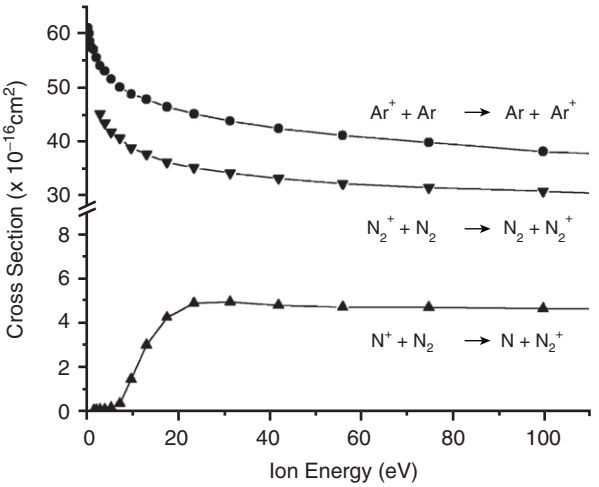


sp0020 **Figure 2.3: Cross-section for the charge exchange reaction of $Ar^+$ ions in argon and $N^+$ and $N_2^+$ ions in nitrogen. (From [10].)**

primary collision processes are momentum exchange ($\sigma_{elastic}$) and, to a lesser degree, excitation ($\sigma_{ex}$). At energies considerably larger than the ionization potential, the primary process is ionization ($\sigma_{ion}$). Note that in electronegative gases like oxygen [7], the halogens, or compounds containing either (e.g. NO, CO, $CO_2$, $CF_4$, $SiF_4$, $SF_6$) [8, 9], electron attachment at lower energies is significant and should not be neglected.

p0215 Cross-sections are most easily measured for reactions involving a species such as an electron or ion, which can conveniently be formed as an energetic beam and passed through a stationary gas. Figure 2.3 shows the charge transfer cross-sections for energetic ions passing through their parent gas [10]. Note in comparing Figures 2.2 and 2.3 that the collision cross-sections are typically on the order of $10^{-16}$ to $10^{-15}$ $cm^2$ (i.e. a few to tens of angstroms in diameter) in magnitude. For collision types that cannot be investigated in beam experiments, typically those that occur at low projectile energies, the cross-sections are often deduced from measurements of macroscopic parameters such as viscosities, diffusion coefficients, drift velocities, and chemical reaction rates [11]. Thus, one finds reference to viscosity cross-sections, diffusion cross-sections, etc. Swarm experiments are a common approach to such measurements, where a swarm of particles is produced in a gas background that is subject to an electric field. These macroscopic parameters or transport coefficients are then measured as a function of the applied electric field. In general, the cross-sections can be calculated using the transport coefficients and vice versa [12, 13]. Depending on the type of analysis or calculation, either the cross-sections or transport coefficients are used. In plasma modeling using fluid approaches [14], one would use transport coefficients, while cross-sections would be better suited to kinetic treatments.

ISBN: 978-0-8155-2031-3; PII: B978-0-8155-2031-3.00002-8; Author:Martin; Document ID:00002; Chapter ID:c0010

st0030 ### *2.2.2 Electron Kinetic Energy*

p0220 As noted, the electron energy can greatly exceed the energy of the gas background. The term 'non-equilibrium' is often used to describe such plasmas. To understand how this occurs, consider an electron elastically colliding with a heavy particle at rest. Using the conservation of energy and momentum, it can be shown that the maximum loss of electron energy in such a collision is [15]:

$$\Delta W = W_{ei} - W_{ef} = (4m_e/M)W_{ei} \tag{2.3}$$

where $m_e$ and $M$ are the electron and heavy-particle masses and $W_{ei}$ and $W_{ef}$ are the electron energies before and after the collision. Equation (2.3) indicates that only a small fraction of the electron kinetic energy is lost in such collisions. For a collision between an electron ($m = 1/1836$ amu) and an argon atom ($M = 40$ amu), the fraction is $\approx 5 \times 10^{-5}$.

p0225 Now consider a plasma electron in an electric field $E$. Between collisions with the gas particles, the electron will gain an energy $W_E$ from the electric field that is equal to the force on the electron $F = qE$ (where $q$ is the electronic charge) times the distance that it moves in the electric field. This distance can be approximated by the mean free path so that, on average, $W_E = qE\lambda$. For a plasma at steady state, this electron energy gained must be balanced against the energy lost in collisions. Considering only elastic collisions, we equate $\Delta W$ in Eq. (2.3) to the energy $W_E$ gained, and using Eq. (2.1) for $\lambda$, yields

$$W_{ei} = (M/2m_e)(qE/N\sigma_{elastic}) \tag{2.4}$$

Equation (2.4) shows that the electron energies can be very large. For the case of electrons in an Argon plasma at 1 torr and 300 K which is subjected to an electric field of 1 V/cm, $N = 3 \times 10^{16}$ cm$^{-3}$ and $qE$ is 1 eV/cm. Using $\sigma_{elastic} \approx 10^{-15}$ cm$^{-2}$ from Figure 2.1, Eq. (2.4) yields $W_{ei} \sim 10^3$ eV. Thus, at steady state, the average electron energy will be much greater than that of the gas atoms, which is approximately 0.039 eV at 300 K. The actual average electron energy will not reach $10^3$ eV, however, because we have neglected other energy sinks. Nevertheless, the above analysis shows that even weak electric fields can cause electron kinetic energies in low-pressure glow discharge plasmas to be elevated well above gas particle energies.

p0230 On the other hand, if the plasma was generated in one atmosphere of argon (760 torr or $N = 3 \times 10^{19}$ cm$^{-3}$), we find $W_{ei} \sim 1$ eV. In other words, collisions are so frequent in high-pressure plasmas that the electron energies are not as high. Moreover, electron/gas particle collisions are so frequent that the gas temperature increases. This behavior is illustrated in Figure 2.4 for the case of plasma arcs (the energies here are expressed as 'temperatures' in eV). When the electron and gas temperatures are the same, the term 'equilibrium plasmas' is often used. High-pressure plasmas, such as arcs or dielectric barrier

ISBN: 978-0-8155-2031-3; PII: B978-0-8155-2031-3.00002-8; Author:Martin; Document ID:00002; Chapter ID:c0010

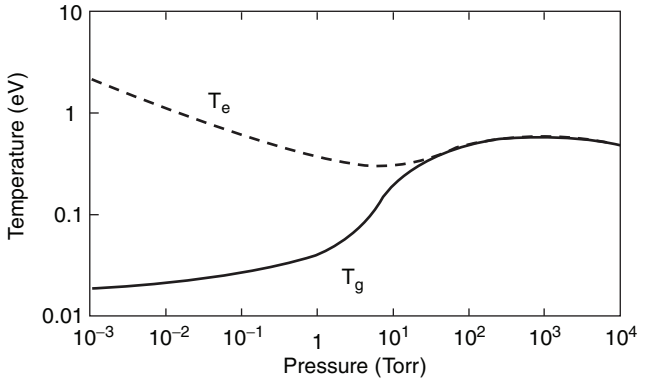


sp0025 **Figure 2.4: Electron ($T_e$) and gas temperatures ($T_g$) in an arc produced in an air background as a function of pressure. (Adapted from [17].)**

discharges [16], are used for a variety of applications. However, the discussion in the following sections will be limited to the low-pressure case where $T_e > T_g$. In this situation, energetic electrons can produce high-temperature chemistry in low-temperatures gases [17, 18], which is an important factor when considering the use of plasmas to promote unique gas-phase chemistries. Indeed, an energy of 1 eV is equivalent to a temperature of about 11,600 K.

st0035 ### 2.2.3 Electron Energy Distribution

p0235 For most purposes, the state of a glow discharge plasma can be characterized by the densities of heavy particles $N_j$, where $j$ corresponds to the $j$th species, the electron density $n_e$, and the electron energy distribution function $F_e(E)$ [19]. Under conditions of local thermodynamic equilibrium [20], when the forward and reverse rates for all the electron energy exchange processes are equal (state of detailed balance) [21], the electrons will have a Maxwellian velocity distribution and their state can be defined by an electron temperature $T_e$. This is overly simplified since a state of equilibrium seldom exists in low-pressure discharge plasmas. It is, nonetheless, a common assumption.

p0240 Figure 2.5 schematically illustrates the electron energy distribution function. For a given Maxwellian energy distribution, the effect of an electric field is to increase the electron energies, thereby shifting the Maxwellian distribution toward higher energies. Elastic collisions, mainly electron–electron, tend to drive the distribution toward lower energies. In fact, electron–electron collisions tend to smooth the distribution and drive it toward the Maxwellian form. Inelastic collisions, on the other hand, will significantly alter the shape of the distribution, making it less Maxwellian. [The cross-section for a representative inelastic collision (ionization) is shown superimposed.] Electrons undergoing inelastic collisions will lose nearly all of their energy and are thus transferred out of the high-energy end of the

ISBN: 978-0-8155-2031-3; PII: B978-0-8155-2031-3.00002-8; Author:Martin; Document ID:00002; Chapter ID:c0010

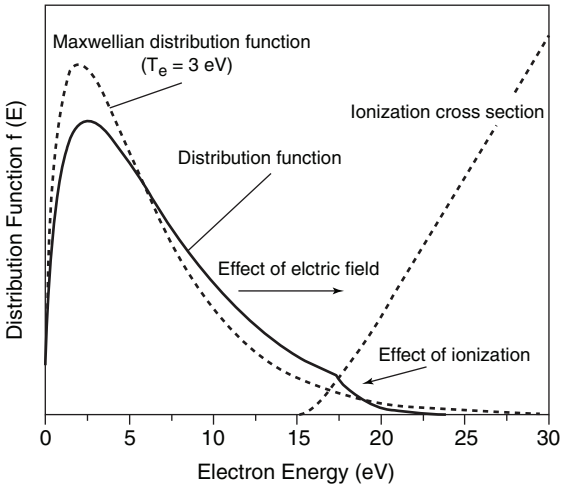


sp0030 **Figure 2.5: Schematic illustration of electron energy distribution function and inelastic (ionization) collision cross-section in argon. The applied electric fields tend to increase electron energies while inelastic collision will depopulate the higher energy electrons. Electron–electron collisions tend to drive the distribution toward a Maxwellian shape.**

distribution. How these influence the shape of the distribution will depend on the type of inelastic collision. Excitations are dominant at low energies, particularly in molecular gases, while ionization dominates at high energies (see Figure 2.2 and Section 2.2.1). The shape of the distribution function has been shown to have a dependence on operating pressure and driving frequency [22] as well as power deposition [23] in low-pressure radio frequency (RF) power-driven plasmas. It is interesting to note that the electron temperature is established to balance the ionization and loses, thus for systems of comparable operating conditions (pressure, gas composition, size, and power), the electron temperature is not dependent on the source of electric power (i.e. RF, DC, microwave, etc.) [24].

p0245 Since, in practice, Maxwellian distributions are often assumed, it is common to use the electron temperature to describe the electrons. This assumption is best when the plasma electrons are collisional; that is, elastic electron collisions dominate and so the electric field perturbation is minimal. Such is the case for high-pressure discharges. The assumption is not as good in low-pressure discharges, where electron–electron collisions are not as significant as the electric field perturbation and the influence of inelastic collisions. In fact, it is not uncommon to find distributions that are bimodal (two peaks in the distribution). Bimodal distributions are often observed in low-pressure negative glow discharges of the type used in sputtering [25].

p0250 Electron energy distribution functions are usually measured by probe methods [26]. However, interpretation of the results is complicated, particularly in multicomponent plasmas [27] typically used in processing. There is a significant body of work concerning the use of probes

ISBN: 978-0-8155-2031-3; PII: B978-0-8155-2031-3.00002-8; Author:Martin; Document ID:00002; Chapter ID:c0010

in the literature and the interested reader should refer to this when performing such measurements. When great care is taken, the electron temperatures derived from probe measurements, although not strictly valid, are a reasonable approximation and can be used to describe the state of the plasma.

st0040 ### 2.2.4 Collision Frequencies

p0255 The collision frequency is an important plasma parameter and is defined as the rate at which an average particle undergoes collisions of a specified type. The total electron–neutral collision frequency is the rate at which an average electron in a plasma undergoes collisions of all types with gas atoms and molecules. The general expression for the collision frequency $\nu$ is rather complex and involves the distribution functions of the colliding species [28]. For the electron–neutral case, the velocity of the heavy particles can be neglected and $\upsilon$ is given by

$$\upsilon_k = N \int_{E=0}^{E=\infty} (E/2m_\mathrm{e})^{1/2} \sigma_k(E) F_\mathrm{e}(E) dE \tag{2.5}$$

where $k$ is the type of collision (e.g. elastic, excitation, ionization, etc). If the collision cross-section $\sigma_k(E)$ is assumed to be independent of energy and the electrons are assumed to have a Maxwellian distribution at an electron temperature $T_\mathrm{e}$, then Eq. (2.5) reduces to

$$\upsilon_k = N \sigma_k \upsilon_e \tag{2.6}$$

The average electron speed $\upsilon_\mathrm{e}$ is

$$\upsilon_\mathrm{e} = (8\mathrm{k}T_\mathrm{e}/\pi m_\mathrm{e})^{1/2} \tag{2.7}$$

where k is Boltzmann's constant. It is customary to write $\mathrm{k}T_\mathrm{e}$ in units of eV.[2] Thus, Eq. (2.7) becomes

$$\upsilon_\mathrm{e} = (6.7 \times 10^7)[\mathrm{k}T_\mathrm{e}(\mathrm{eV})]^{1/2}\ \mathrm{cm/s} \tag{2.8}$$

Because the velocity is determined using $\mathrm{k}T_\mathrm{e}$, $\sigma_k$ in Eq. (2.6) is also approximated by its value at the electron energy $\mathrm{k}T_\mathrm{e}$. The electron–electron and electron–ion collision frequencies are of special interest. These are given by [29, 30]:

$$\upsilon_\mathrm{ee} = (3 \times 10^{-6}) n_\mathrm{e} \ln\Lambda / [\mathrm{k}T_\mathrm{e}(\mathrm{eV})]^{3/2}\ \mathrm{s}^{-1} \tag{2.9}$$

[2] In kinetic theory, the average particle energy $E$ is related to the gas temperature $T$ and so it is customary in plasma physics to give temperature in units of eV. The average particle energy in one dimension is properly defined as 1/2 k$T$, while the average energy in three dimensions is 3/2 k$T$. However, it is not the average energy but, rather, the energy corresponding to k$T$ that is used to denote the temperature. By a 2 eV plasma, we mean that k$T$ = 2 eV, although the actual average energy in three dimensions is 3/2 k$T$ or 3 eV.

ISBN: 978-0-8155-2031-3; PII: B978-0-8155-2031-3.00002-8; Author:Martin; Document ID:00002; Chapter ID:c0010

and

$$\nu_{ei} = (1.5\times10^{-6}) n_e \ln\Lambda/[kT_e(eV)]^{3/2}\ s^{-1} \tag{2.10}$$

with

$$\lambda_{ee} = (4.5\times10^{13})[kT_e(eV)]^2/(n_e \ln\Lambda)\ cm \tag{2.11}$$

where $\ln\Lambda$ is a weak function of $kT_e$ and $n_e$. The $\ln\Lambda$ term arises to correct for the infinite nature of collisions involving long-range coulomb forces. In a plasma, the presence of other charged species effectively shields charged particles from the influence of those outside a characteristic distance and so there can be no long-range coulomb forces. This characteristic distance is defined as the Debye length (see Section 2.3). The function $\ln\Lambda$ is tabulated in some books on plasma physics [31, 32], and has a value in the range of 10–15 for discharge plasmas of interest in this chapter.

p0260 It is useful to compare the electron collision frequencies of Eqs. (2.9) and (2.10) with other relevant collision frequencies. A plasma for which $\nu_{ee} > \nu_{eA}$, where $\nu_{eA}$ is the elastic electron–atom collision frequency, is said to be coulomb dominated. An approximate condition for coulomb domination is easily derived from Eqs. (2.6) and (2.9) [31]:

$$\frac{n_e}{N} \gg \alpha_c = (2.23\times10^{13})\frac{\sigma_{eA}[kT(eV)]^2}{\ln\Lambda} \tag{2.12}$$

The term $\alpha_c$ in Eq. (12) is known as the critical degree of ionization. Selecting $kT_e \approx 3$ eV and $\sigma_{eA} \sim 10^{-15}\ cm^{-3}$ (Figure 2.1) yields $n_e/N \approx 0.02$. Thus a moderate-temperature glow discharge plasma with 2% ionization can be dominated by coulomb collisions.

p0265 A consequence of coulomb domination can be seen by examining Eqs. (2.9) and (2.11). As the electron energy is increased, the electron collision frequency decreases and the mean free path will increase. Thus, electrons in an electric field will find that their energy gain is not clamped by collisions. Electron runaway is an important consideration in highly ionized plasmas [33] but seldom important in glow discharge plasmas because of inelastic collisions.

p0270 For heavy particle collisions, collision frequency can be approximated by an equation very similar to Eq. (2.6) [15, 34]. For the case of a heavy particle of mass $M_k$ in a gas with density $N_j$ of heavy particles of mass $M_j$, the collision frequency is given by

$$\nu_{kj} \approx (2.5\times10^{5})\frac{(\sigma N)_{kj}}{(M*)^{1/2}}\left[\frac{T}{300}\right]^{1/2} \tag{2.13}$$

ISBN: 978-0-8155-2031-3; PII: B978-0-8155-2031-3.00002-8; Author:Martin; Document ID:00002; Chapter ID:c0010

where the cross-section is assumed to be independent of the velocity of impact and all the heavy particles are at the common temperature $T$. In Eq. (2.13) $M^*$ is a reduced mass defined as

$$M^* = \frac{M_k M_j}{M_k + M_j} \tag{2.14}$$

where the masses are molecular weights expressed in grams.

st0045 ### 2.2.5 Reaction Rates

p0275 The gas-phase reaction rate R is directly proportional to the collision frequency. For a process k involving electron collisions,

$$R_k = n_e v_k \text{ cm}^{-3} \text{ s}^{-1} \tag{2.15}$$

If the electrons are assumed to have a Maxwellian velocity distribution at a temperature $T_e$, and if the cross-section for a given reaction is approximated by a step function of magnitude $\sigma_o$ and threshold energy $E_o$ as shown in Figure 2.6, then the reaction rate is given by

$$R_k = n_e N \sigma_o v_e [1 + (E_o / kT_e)] \exp(-E_o / kT_e) \tag{2.16}$$

For reactions involving heavy particle collisions, reaction rate constants rather than actual collision frequencies are typically measured and used. For a reaction occurring via a two-body

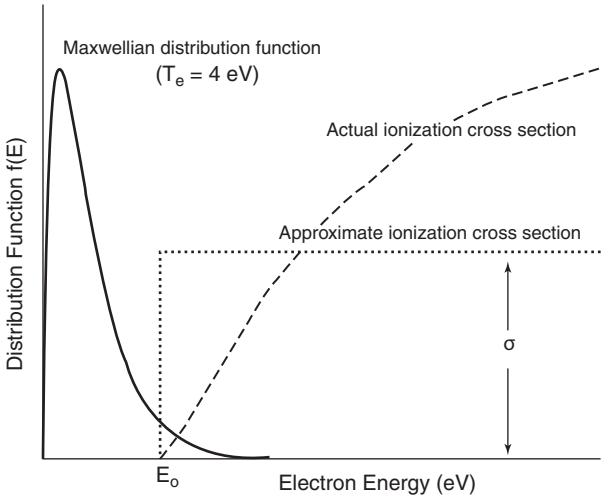


sp0035 **Figure 2.6: Ionization reaction rate approximation for a Maxwellian electron energy distribution.**

ISBN: 978-0-8155-2031-3; PII: B978-0-8155-2031-3.00002-8; Author:Martin; Document ID:00002; Chapter ID:c0010

sp0165 **Table 2.1: Charge exchange reactions and the associated reaction rate constants $\kappa(T)$ at 293 K**

| Reaction | Rate constant ($cm^3$/mol·s) |
|---|---|
| $Ar^+ + Ar \rightarrow Ar + Ar^+$ | $4.6 \times 10^{-10}$ |
| $Ar^+ + N_2 \rightarrow Ar + N_2^+$ | $1.3 \times 10^{-11}$ |
| $Ar^+ + O_2 \rightarrow Ar + O_2^+$ | $4.9 \times 10^{-11}$ |
| $Ar^+ + H_2 \rightarrow H + ArH^+$ | $8.9 \times 10^{-10}$ |
| $N^+ + N_2 \rightarrow N_3^+$ | $1.3 \times 10^{-13}$ |
| $N_2^+ + N_2 \rightarrow N + N_3^+$ | $2.8 \times 10^{-12}$ |
| $N_2^+ + O_2 \rightarrow N_2 + O_2^+$ | $8.5 \times 10^{-11}$ |
| $N_2^+ + Ar \rightarrow N_2 + Ar^+$ | $1.0 \times 10^{-13}$ |
| $O^+ + O_2 \rightarrow O + O_2^+$ | $2.2 \times 10^{-11}$ |
| $O_2^+ + N_2 \rightarrow NO + NO^+$ | $2.0 \times 10^{-18}$ |
| $CH_4^+ + CH_4 \rightarrow CH_5^+ + CH_3$ | $1.2 \times 10^{-9}$ |

sp0170 *From [35].*

collision between species $i$ and $j$ in a gas at temperature $T$, with rate constant $\kappa(T)$, the rate is

$$R = \kappa(T) N_i N_j \tag{2.17}$$

Table 2.1 gives the rate constants for various charge transfer processes.

st0050 ### 2.2.6 Mobilities

p0280 Plasma transport properties are dependent on the frequency of elastic (momentum exchange) collisions. The mobility $\mu_j$ relates the electric-field driven drift velocity $v_d$ of a given charged particle species $j$ to the strength of the field $E$:

$$v_{dj} = \mu_j E \tag{2.18}$$

When the collision frequency is sufficiently large that the drift velocity is small compared to the thermal velocity,

$$\mu_j = \frac{1.6 \times 10^{-12}}{m_j v_{ji}} \tag{2.19}$$

where $m_j$ is the particle mass in grams.

p0285 The mobility is generally used to describe the drift of ions through a plasma that is at a sufficiently high pressure to satisfy the collision frequency requirement ($v_{th} > v_d$). Reduced mobilities for several gases of interest are given in Table 2.2.

p0290 When a positive ion collides with a gas molecule or atom, two processes can occur. First, the

ISBN: 978-0-8155-2031-3; PII: B978-0-8155-2031-3.00002-8; Author:Martin; Document ID:00002; Chapter ID:c0010

sp0175 **Table 2.2: Reduced mobilities of ions in their own gas for a vanishing electric field**

| Ion–Gas | $\mu_{jo}$ (cm$^2$/V·s) |
|---|---|
| $He^+$–He | 10.3 |
| $Ne^+$–Ne | 4.08 |
| $Ar^+$–Ar | 1.52 |
| $O_2^+$–Ar | 2.57 |
| $O^+$–Ar | 3.43 |
| $H^+$–$H_2$ | 16.0 |
| $H^-$–$H_2$ | 42.7 |
| $N_2^+$–$N_2$ | 1.90 |
| $N^+$–$N_2$ | 3.01 |
| $O_2^+$–$O_2$ | 2.23 |
| $O^-$–$O_2$ | 3.20 |

sp0180 *From [36].*

sp0185 *Conditions are: P = 760 torr, T = 300 K, E = 0. Thus, $\mu_j = K\mu_{jo}$, where K = (760/P)(T/300).*

ion and molecule can exchange momentum and energy in a collision. Second, an exchange of charge can occur. For example, fast ions colliding with slow neutrals can extract an electron from the slow neutral. After the exchange, the fast ion becomes a fast neutral while the slow neutral becomes a slow positive ion. For ions drifting through a gas at room temperature, repeated charge exchange collisions can effectively behave as though a single ion undergoes repeated collisions in which the ion loses all of its kinetic energy [37]. Resonant charge exchange, where the ion and neutral are identical (with the exception of charge), is an important consideration. For this process, the cross-section increases with decreasing ion energy (see Figure 2.3) and at low ion energies, is about one-half of the total cross-section [38]. Thus, resonant charge exchange contributes significantly to determining the mobility of ions drifting through their parent gas. Charge transfer is very important in high-pressure sputtering and ion-plating discharges where collision frequencies are high.

st0055 ### 2.2.7 Conductivity and Diffusion

p0295 The electrical conductivity $\sigma$ is just $qN\mu$, so that

$$\sigma_j = 1/\rho_j = 2.6\times10^{-31}(N_j/m_j\nu_{ji})\,(\mathrm{Wcm})^{-1} \tag{2.20}$$

where $N_j$ is the particle density in cm$^{-3}$ and $m_j$ is the mass of the current carrier in grams. Since $\sigma$ is the common symbol for both the electrical conductivity and the collision cross-section, the resistivity $\rho$ is often used to avoid confusion.

p0300 The diffusion coefficient $D$ relates the particle flux $\Gamma$ to the density gradient. Thus, one has

$$\Gamma_j = N_j\upsilon_{dj} = D_j(dN_j/dx) \tag{2.21}$$

ISBN: 978-0-8155-2031-3; PII: B978-0-8155-2031-3.00002-8; Author:Martin; Document ID:00002; Chapter ID:c0010

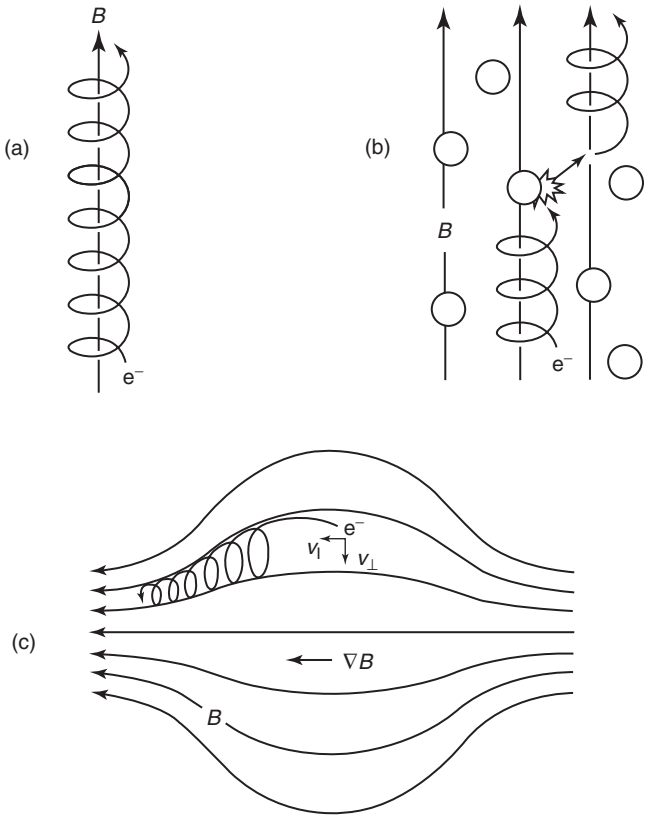


sp0040 **Figure 2.7: Electron paths in static magnetic fields.**

where

$$D_j = \frac{kT}{m_j \upsilon} = (1.6\times10^{-12})\frac{kT(\text{eV})}{m_j \upsilon} \ \text{cm}^2/\text{s} \tag{2.22}$$

This description of diffusion neglects the interaction of oppositely charged species and is thus often referred to as free diffusion. Ambipolar diffusion describes the diffusion of charged species and is covered in Section 2.3.2.

st0060 ### *2.2.8 Particle Motion in Magnetic Fields*

p0305 The force exerted on a charged particle in a magnetic field is given by $F_B = q(\nu \times B)$ and affects the motion of a particle in ways that are summarized in Figure 2.7. A charged particle in a uniform magnetic field $B$ will orbit a field line as shown in Figure 2.7(a) while drifting along the field with parallel velocity $v_{||}$ that is unaffected by the field. The orbiting frequency

ISBN: 978-0-8155-2031-3; PII: B978-0-8155-2031-3.00002-8; Author:Martin; Document ID:00002; Chapter ID:c0010

is called the gyro or cyclotron frequency and is given by

$$\omega_c = eB/m \tag{2.23}$$

The orbiting radius is called the gyro, cyclotron, or Larmor radius and is given by

$$r_g = (m/3)(\upsilon_\perp/B) \tag{2.24}$$

p0310 There are a few points to consider when using magnetic fields in plasma processing systems. First, the use of magnetic fields to manipulate and confine plasmas requires that $r_g$ be small compared to the critical apparatus size such as the chamber dimensions, electrode separations, or substrate locations. Note that $r_g$ depends directly on the mass of the particle and so much larger magnetic fields are required to influence the motions of the plasma ions compared to the electrons. For particles of the same velocity subject to a given field, the ion gyro radius will be at least three orders of magnitude greater than the electron gyroradius. With this in mind, magnetic fields are generally chosen to be strong enough to influence the plasma electrons, not the ions. However, since electrostatic forces prevent the ions from escaping from the electrons, magnetically confined electrons in a discharge will provide considerable confinement for the plasma ions. Magnetic field strengths between 200 and 300 gauss are common in magnetrons.

p0315 For electrons, Eqs. (2.23) and (2.24) become

$$\omega_c = (1.76\times10^7)\, B\,\text{rad/s} \tag{2.25}$$

where $B$ is in gauss, and

$$r_g = 3.37\ \frac{W_\perp}{B}\,\text{cm} \tag{2.26}$$

where $W_\perp$ is in eV. Thus, for electrons with an average energy $W_\perp$ of 10 eV and a magnetic field strength $B$ of 100 G, the gyro radius is $\approx 0.1$ cm. For $Ar^+$ ions of the same energy, the gyro radius is $\approx 270$ cm. Recall, however, the energy of ions in the bulk plasma are typically in thermal equilibrium with the surrounding gas and so have a much lower energy than the electrons. In that case, the gyro radius is approximately 15 cm, still significantly larger than the electrons.

p0320 An electron that is trapped on a given magnetic field line can advance to an adjacent field line after colliding with a larger species, as indicated schematically in Figure 2.7(b). Collisional diffusion of electrons across magnetic field lines is an important consideration in many discharge devices.

ISBN: 978-0-8155-2031-3; PII: B978-0-8155-2031-3.00002-8; Author:Martin; Document ID:00002; Chapter ID:c0010

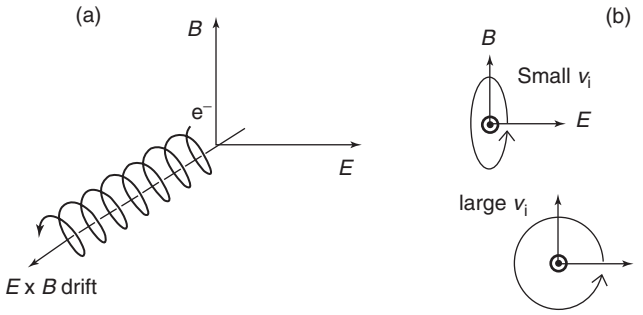


sp0045 **Figure 2.8: Electron paths in static magnetic and electric fields.**

p0325 The drift of electrons along a magnetic field line can also be influenced by gradients in the magnetic field. An example of this behavior is shown in Figure 2.7(c), for a 'pinched-field' arrangement often used in discharge devices. In this configuration, the field strength increases as the field pinches (field lines get closer), and so $\omega_g$ increases while $r_g$ remains fixed because electrons moving in such a field tend to conserve the magnetic moment, $\mu_M$, defined by [29]

$$\mu_M = W_\perp / B \tag{2.27}$$

Thus, $W_\perp$ must increase as the electrons move in the direction of increasing field strength. Conservation of energy requires that $W_{||} + W_\perp$ be constant. Therefore $W_{||}$ must decrease, so that electrons will slow and will likely be reflected.

p0330 When both electric and magnetic fields are present, the electrons are subject to the forces of both, as shown in Figure 2.8. When the electric field $E$ is directed parallel to the magnetic field $B$, the electrons are freely accelerated along the field lines. However, if the electric field has a component $E_\perp$ which is perpendicular to $B$, the electrons undergo a drift in a direction perpendicular to both $E_\perp$ and $B$, as shown in Figure 2.8(a). This motion is known as the $E \times B$. The motion is cycloidal if the initial electron energy is small compared to that gained from the electric field; it has the more circular form if the initial electron energy is large compared to the electric-field-induced variations that occur during the course of the orbit (Figure 2.8b). In both cases, the electron drift speed is given by

$$\upsilon_e = 108 \frac{E_\perp}{B} \text{ cm/s} \tag{2.28}$$

with $E_\perp$ in V/cm and $B$ in gauss.

## st0065 2.3 Plasma Parameters and Collective Behavior

p0335 Plasmas differ from non-ionized gases by their propensity for undergoing collective behavior associated with the interaction of charged species as well as the mass and energy difference

ISBN: 978-0-8155-2031-3; PII: B978-0-8155-2031-3.00002-8; Author:Martin; Document ID:00002; Chapter ID:c0010

between the charged particles. Three parameters: the Debye length $\lambda_D$, plasma frequency $f_p$, and critical degree of ionization $\alpha_c$, provide a useful measure of the tendency toward collective behavior. These parameters are derived from basic plasma properties of gas density $N$, electron density $n_e$, and electron energy $T_e$.

p0340 The Debye length corresponds to the distance in which significant departures from charge neutrality occurs and is given by

$$\lambda_D = 743\left[\frac{kT_e}{n_e}\right]^{1/2} \text{cm} \tag{2.29}$$

with $kT_e$ in eV and $n_e$ in $cm^{-3}$. This characteristic length defines a plasma; one cannot exist in a space having dimensions less than $\lambda_D$.

p0345 The plasma frequency provides a measure of the tendency for electrostatic waves to develop and is expressed here as

$$f_p = \omega_p/2\pi = 9000[n_e]^{1/2}\,\text{Hz} \tag{2.30}$$

Waves can form if $\omega_p \gg \nu_{e,\,\text{elastic}}$ where $\nu_{e,\,\text{elastic}}$ is the electron collision frequency for momentum exchange. The inverse of $f_p$ defines the characteristic time of the waves.

p0350 The critical degree of ionization $\alpha_c$ was defined by Eq. (2.12) and is listed again for completion:

$$\alpha_c = (2.23\times10^{13})\frac{\sigma_{eA}[kT(\text{eV})]^2}{\ln\Lambda}$$

p0355 When the degree of ionization $\alpha = n_e/N$ is much greater than $\alpha_c$, coulomb collisions dominate, and the charged particles behave as though they were in a fully ionized gas. This can occur at degrees of ionization of a few percent for plasmas with low average electron energies ($\approx$1 eV).

st0070 ### 2.3.1 Plasma Sheaths

p0360 Given a gas of particle density $N$ and temperature $T$, the flux of particles passing to an adjacent wall is given by

$$\Gamma = n\upsilon/4 = (n/4)(8kT/\pi m)^{1/2} \tag{2.31}$$

For electrons, this becomes (see Eqs. 2.7 and 2.8)

$$\Gamma_e = (1.67\times10^7)n_e[kT_e(\text{eV})]^{1/2}\,\text{cm}^{-2}\,\text{s}^{-1} \tag{2.32}$$

ISBN: 978-0-8155-2031-3; PII: B978-0-8155-2031-3.00002-8; Author:Martin; Document ID:00002; Chapter ID:c0010

which, in units of current density, is equal to

$$J_e = (2.7\times10^{-9})n_e[kT_e(eV)]^{1/2}\ \text{mA/cm}^2 \tag{2.33}$$

Thus, for a discharge with a electron density of $10^{10}\ \text{cm}^{-3}$ and an average energy of 4 eV, $J_e \approx 60\ \text{mA/cm}^2$.

p0365 For heavy particles such as ions, Eq. (2.31) can be written in the following useful form:

$$\Gamma_i = 10^4 n_i(40/M)^{1/2}(T/300)^{1/2} \tag{2.34}$$

where $T$ is the gas temperature in Kelvin and M is the species molecular weight. In units of current density, Eq. (2.34) becomes

$$J_i = 1.6\times10^{-12}n_i(40/m)^{1/2}(T/300)^{1/2}\ \text{mA/cm}^2 \tag{2.35}$$

Thus, for a plasma produced in argon with an ion density of $10^{10}\ \text{cm}^{-3}$ at 300 K, the ion current to the wall is $J_i \approx 1.6 \times 10^{-2}\ \text{mA/cm}^2$.

p0370 The ratio of ion to electron fluxes (from Eq. 2.31) gives

$$\frac{\Gamma_i}{\Gamma_e} = \frac{n_e(kT_i/m_i)^{1/2}}{n_i(kT_e/m_e)^{1/2}}$$

For a plasma in quasiequilibrium ($n_e \approx n_i$) and writing the masses in atomic mass units, Eq. (2.35) reduces to

$$\frac{\Gamma_i}{\Gamma_e} = \frac{1}{\sqrt{1836}}\sqrt{\frac{T_i}{T_e m_i(A)}}$$

It is clearly seen that the electrons tend to flow from a plasma to an adjacent wall at a faster rate than the ions. For an argon plasma where the electron temperature is 4 eV and the ions are at room temperature, $\Gamma_i/\Gamma_e \approx 3 \times 10^{-4}$. Because of this significant difference, a space charge region in which one species is largely excluded forms adjacent to such surfaces. These regions are called sheaths, and are typically several Debye lengths in thickness.

p0375 The nature of the sheath will depend on the current density passing across it. Except for cases involving very high current densities to anodes, the sheath will contain primarily the low-mobility ion species, and such sheaths are known as positive space charge sheaths or simply ion sheaths. This causes a potential to develop across the sheath, called the sheath potential or sheath drop, which forms a barrier capable of reflecting the more mobile electrons (except in the case of a strong magnetic field). The sheath potential adjusts itself so that the flux of electrons to the wall equals the electron current that is drawn from the wall by the external circuit. If the wall is electrically isolated, the electron flux is reduced to the point

ISBN: 978-0-8155-2031-3; PII: B978-0-8155-2031-3.00002-8; Author:Martin; Document ID:00002; Chapter ID:c0010

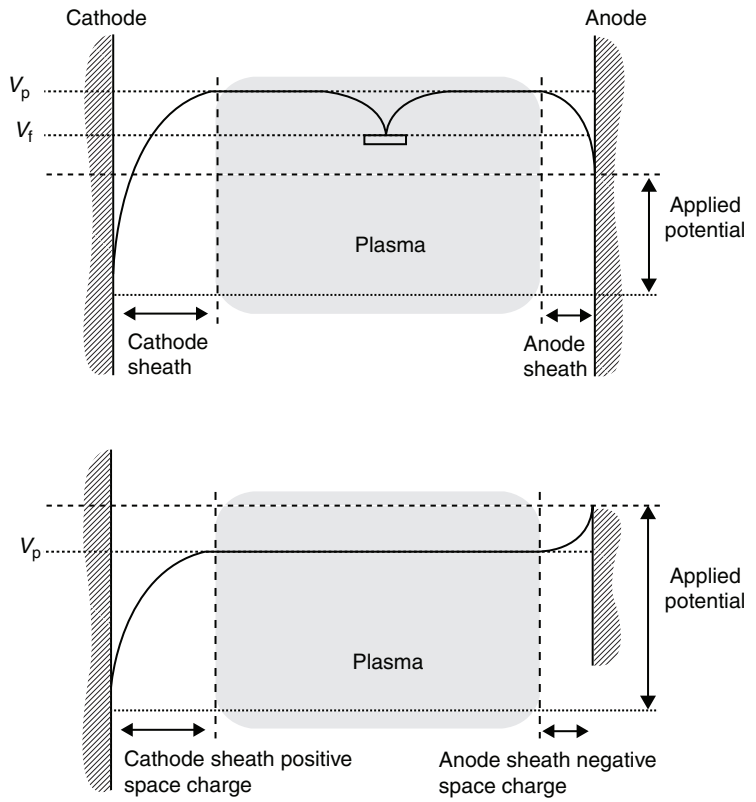


sp0050 **Figure 2.9: Schematic illustration of sheaths that form between a plasma discharge and the surrounding apparatus walls for systems having (a) a large anode and (b) a small anode. Also shown in (a) is a floating metal surface immersed in plasma.**

which is equal to the ion flux. It is intuitive to note the importance of the sheath. Indeed, without it, the quasi-neutrality of the plasma is in jeopardy.

p0380 Figure 2.9 shows a schematic illustration of a typical discharge plasma which is in contact with surfaces that are either cathodes or anodes, or electrically isolated (floating). The plasma potential $V_p$ forms with respect to the most positive surface (anode) [39]. The potential of a floating surface relative to the plasma potential is known as the floating potential $V_f$. For a Maxwellian energy distribution, the floating potential is given by [40]:

$$V_f = \frac{kT_e(eV)}{2e} \ln\left[\frac{\pi m_e}{2m}\right] \tag{2.36}$$

This is the potential with respect to the plasma potential and thus, when a floating surface is immersed in a plasma, the surface will be bombarded with ions having kinetic energies of up to $-e(V_p - V_f)$. The natural log term in Eq. (2.36) is typically on the order of 10 for most

ISBN: 978-0-8155-2031-3; PII: B978-0-8155-2031-3.00002-8; Author:Martin; Document ID:00002; Chapter ID:c0010

discharges used in processing and so $V_f$ scales with electron temperature. Thus, values for $V_f$ will be in the range 5–50 V.

p0385 In general, the anodes used in discharges are large enough that the current density is less than the current driven by $T_e$ (Eq. 2.33). In this case, the plasma potential is above the anode potential (Figure 2.9a), there is a positive space charge sheath at the anode, and the sheath potential drop is between zero and $-(V_p - V_f)$. On the other hand, if the anode area is so small that the current density must exceed the $T_e$-driven current, then the anode potential will be above the plasma potential, as shown in Figure 2.9(b). The local electric field surrounding the anode will draw sufficient electrons to the anode to supply the external circuit.[3]

p0390 A large potential difference $V_{s,}$ approximately equal to the entire potential applied by the power supply, occurs in the cathode sheath as shown schematically in Figure 2.10. The sheath thickness $d_s$ is taken to be the region over which the full potential drop $V_s$ occurs. Over the sheath thickness, the electron density is negligible. For the low-pressure case, where the ion mean free path is larger than $d_s$, the ion current density $J_i$ at the wall is related to $d_s$ and $V_s$ by the Child–Langmuir law [29]. It is useful to write this relationship as

$$J_i = 0.273(40/m_i)^{1/2}(V_s^{3/2}/d_s^2)\,\text{mA/cm}^2 \tag{2.37}$$

where $V_s$ is in kV, $d_s$ is in cm, and $M_i$ is the ion mass in u. For an Ar sputtering plasma ($M_i = 40$) with $V_s = 1$ kV and $d_s = 1$ cm, $J_i = 0.27$ mA/cm$^2$. Here we find a higher current than that found earlier (see Eq. 2.35). Thus, the application of an applied bias will increase the current.

p0395 It is difficult to directly relate $J_i$ to the density $N_{io}$ of ions in the bulk plasma, because there is a quasi-neutral presheath region where a potential drop $V_{ps}$ of about $1/2(kT_e/e)$ occurs. However, the presheath density can be assumed to obey a Boltzmann distribution [41], such that $N_{is}/N_{io} = \exp(eV_{ps}/kT_e)$, and the density can be estimated using

$$J_i \approx (9.12\times10^{-11})N_{io}(kT_e/m_i)^{1/2}\,\text{mA/cm}^2 \tag{2.38}$$

where $M_i$ is in u and $kT_e$ is in eV.

p0400 Assuming quasineutrality in the bulk plasma ($N_{io} \approx n_e$), the sheath thickness $d_s$ can be calculated by substituting Eq. (2.38) into Eq. (2.37) and introducing the Debye length from Eq. (2.29). This yields the expression

$$d_s = 185\lambda_D(V/kT_e)^{3/4}\,\text{cm} \tag{2.39}$$

[3] The potential increase at a small anode is largely limited by the ionization potential of the gas atoms. A potential increase of this amount causes the electrons to be accelerated to energies large enough to ionize the gas, which produces additional electrons that can then provide the required anode current. Thus, no additional rise in potential is needed to draw electrons from the plasma.

ISBN: 978-0-8155-2031-3; PII: B978-0-8155-2031-3.00002-8; Author:Martin; Document ID:00002; Chapter ID:c0010

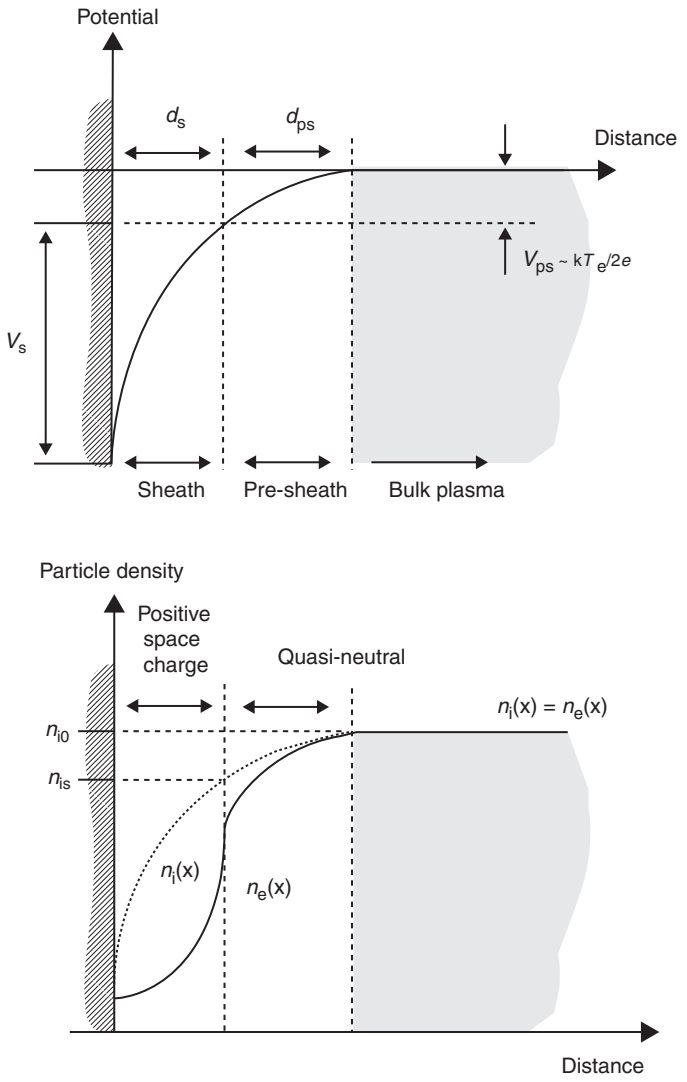


sp0055 **Figure 2.10: Schematic representation of the presheath and sheath that develops at a cathode. The top is the potential profile showing the presheath $V_{ps}$ and sheath $V_s$ potentials. The bottom shows the ion $n_i(x)$ and electron $n_e(x)$ density profiles along with the ion density at the plasma ($n_{io}$) and sheath ($n_{is}$) boundaries.**

For the high-pressure case, where collisions are so frequent that the ion drift velocity is of the order of the thermal velocity, a mobility description is used for the ion motion [17]. Under this condition,

$$J_i = 9.95\times10^{-5}\mu_i(V_s^2/d_s^3)\ \text{mA/cm}^2 \tag{2.40}$$

ISBN: 978-0-8155-2031-3; PII: B978-0-8155-2031-3.00002-8; Author:Martin; Document ID:00002; Chapter ID:c0010

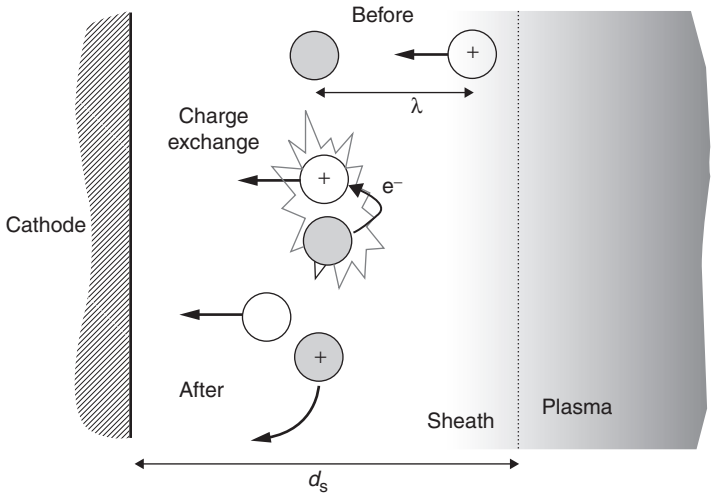


sp0060 **Figure 2.11: Schematic representation of a charge exchange reaction in the sheath, which produces a slow ion and fast neutral. After the collision, the slow ion is accelerated toward the cathode by the electric field in the sheath.**

where $\mu_i$ is the ion mobility in $cm^2$/V-s, $V_s$ is the sheath potential drop in kV, and $d_s$ is the sheath thickness in cm. For an Ar plasma at 1 torr, $\mu_i = 1155\ cm^2$/V-s from Table 2.2. Taking $V = 1$ kV and $d_s = 1$ cm yields $J_i = 0.11\ mA/cm^2$.

p0405 In low-pressure plasmas, where the mean free path for charge exchange is greater than the sheath thickness, the ions will fall through the entire sheath potential and bombard the cathode with a energy about equal to $eV_s$. This is common in deposition processes using magnetrons. At higher pressures, where charge exchange is likely in the sheath, the bombarding flux will consist of both ions and fast neutrals having energies considerably less than $eV_s$ as indicated schematically in Figure 2.11. The resulting ion energy distributions are discussed in Section 2.6.2. Charge exchange in the sheath is an important consideration in DC sputtering applications such as ion plating, high-pressure etching, or PACVD.

st0075 ### *2.3.2 Ambipolar Diffusion*

p0410 The previous discussion of sheath formation to ensure the equal flow of ions and electrons from a plasma can be extended to any region of space. That is, the flow of electrons and ions out of any volume must be equal or an electric field will develop to preserve charge neutrality over that volume. This coupled particle motion is called ambipolar diffusion. The diffusion flux $\Gamma$ of electrons or ions is given by

$$\Gamma_e = D_a(dn_e/dx) = \Gamma_i = D_a(dn_i/dx) \tag{2.41}$$

ISBN: 978-0-8155-2031-3; PII: B978-0-8155-2031-3.00002-8; Author:Martin; Document ID:00002; Chapter ID:c0010

The term $D_a$ is called the ambipolar diffusion coefficient and can be written as

$$D_a = \frac{\mu_i D_e + \mu_e D_i}{\mu_i + \mu_e}$$

Noting that $\mu_e \gg \mu_i$ (see Eq. 2.19) permits $D_a$ to be approximated as [42]

$$D_a \approx D_i(1 + T_e/T_i) \tag{2.42}$$

where $D_i$ is given by Eq. (2.22). Thus, the effect of the ambipolar field is to enhance the diffusion of ions, but the diffusion rate of the two species together is primarily controlled by the slower species.

p0415 In the presence of a sufficiently strong magnetic field perpendicular to the direction of diffusion, the electron mobility can be reduced significantly and it, rather than the ion mobility can become rate limiting ($\mu_e \ll \mu_i$). Under this condition, a form similar to Eq. (2.41) is used,

$$D_{\perp a} \approx \{D_e/[1 + \omega_c^2/\nu_e)]\}(1 + T_i/T_e) \tag{2.43}$$

where $D_e$ is the electron diffusion coefficient in the absence of a magnetic field. The effect of the magnetic field becomes strong when $\omega_e$ (given by Eq. 2.25) is much larger than the electron collision frequency $\nu_e$, i.e. when the electrons are trapped on magnetic field lines as shown in Figure 2.7(a), and collisional hopping to adjacent field lines is infrequent. It should be noted that Eq. (2.42) is based on the assumption that electron losses along the lines can be neglected. Attention to these losses should be given when analyzing the performance of an actual device [29, 43].

st0080 ### 2.3.3 Plasma Oscillations

p0420 The plasma state is rich in wave phenomena when the degree of ionization is large enough to make long-range forces important, particularly when a magnetic field is present [29]. Departures from charge neutrality in the bulk plasma capable of generating waves can occur in the form of charge bunching and separation over distances of the order of the Debye length (Eq. 2.29). A general discussion of such behavior is beyond the scope of this chapter. However, one case will be mentioned because of its potential importance in sputter deposition. Consider the case of a plasma in a uniform electric and magnetic field, as illustrated in the left side of Figure 2.12. There is an $E \times B$ drift perpendicular to both $E$ and $B$, and in the absence of collisions, there should be no transport across the magnetic field in the direction of the applied electric field. If charge bunching occurs, as shown in the right side of Figure 2.12, the perturbation produces a local electric field $E_p$ that can result in $E \times B$ drift across the magnetic field, in a direction parallel to the applied electric field. This anomalous collisionless transport

ISBN: 978-0-8155-2031-3; PII: B978-0-8155-2031-3.00002-8; Author:Martin; Document ID:00002; Chapter ID:c0010

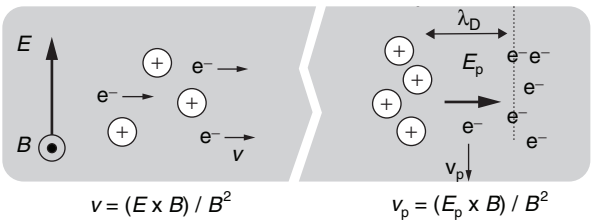


sp0065 **Figure 2.12: Schematic representation of charge neutrality breaking (charge bunching) resulting in electron transport across a magnetic field. The local electric field becomes dominant and causes a change in velocity.**

across the magnetic field is believed to be an important mechanism in Penning discharges as well as in magnetron sputtering discharges [44].

st0085 ## 2.4 Discharge Plasmas

st0090 ### *2.4.1 Introduction*

p0425 A discharge plasma is a low-temperature, relatively low-pressure, gas in which a degree of ionization is sustained by energetic electrons. Discharge configurations used in materials processing differ in their general geometry, the type of applied field, and the orientation of the electric field that is used to provide energy to the electrons. Shown in Figure 2.13 are four general configurations for plasmas driven by AC power. Specific embodiments of these often used in materials processing are further illustrated in Figure 2.14. Discharges driven by DC power are shown in Figures 2.17–2.20.

p0430 In sputtering, simple planar diodes of the type shown schematically in Figure 2.13(a) can be used. They may be driven at radio frequencies (RF), as shown in the figure, or by a DC power supply. Bias sputtering is a common technique for controllably tuning, in real time, the chemistry, phase, microstructure, and, hence, physical properties of growing films. RF planar diode discharges are also used for plasma etching, and reactive ion etching. Systems with the configuration shown in Figure 2.13(d) are also used for PACVD.

p0435 In plasma etching, PACVD, and plasma polymerization, discharges are often sustained in glass or quartz reactor tubes by surrounding electrodes which are driven at high frequencies (from 300 kHz to microwave frequencies) [45]. Common electrode configurations are a pair of ring electrodes along the tube, a solenoidal coil electrode as shown in Figure 2.13(b), or clam-shell electrodes as shown in Figure 2.13(c). Alternatively, the coil could be flat as shown in Figure 2.13(d). It should be noted that all of these discharges are basically capacitive in nature. Although the coil electrode will introduce considerable inductance into the load seen by the matching network, the capacitive fields generated by the coil-to-coil potential drop dominate

ISBN: 978-0-8155-2031-3; PII: B978-0-8155-2031-3.00002-8; Author:Martin; Document ID:00002; Chapter ID:c0010

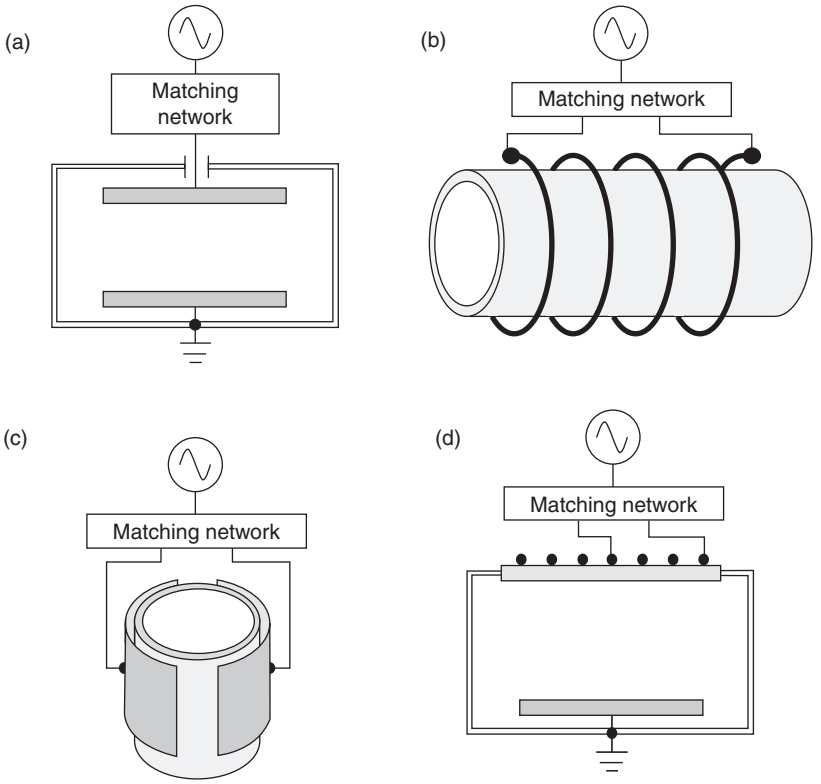


sp0070 **Figure 2.13: Schematic illustrations of generic RF-driven discharge devices. (a) Parallel plate reactor, (b) barrel reactor ICP, (c) clam shell reactor, and (d) flat coil ICP.**

over those generated by the time rate of change of magnetic flux and therefore act as the primary source of ionization unless special precautions are taken to shield them. Inductive sources will be discussed later. In the case of microwave discharges, the reactor tube is generally positioned within the waveguide at a location which places a strong electric field component within the tube [18, 45].

p0440 In ion plating, the discharge is generally sustained in a mixture of the evaporated flux and an inert working gas with the substrate holder biased negatively relative to the plasma potential. Usually this is done by simply making the substrate holder the cathode electrode for sustaining the plasma discharge, as shown in Figure 2.15(a). The ion bombardment of the growing coating has been shown to influence its microstructure [46]. Activated reactive evaporation is a similar approach where a plasma discharge, produced using a variety of electrode configurations driven either by DC or RF power, is sustained in a flux of evaporated material and reactive gas that is directed toward the substrates, as shown in Figure 2.15(b). The presence of the plasma has been shown to influence properties such as the chemical composition of the resultant films [47].

ISBN: 978-0-8155-2031-3; PII: B978-0-8155-2031-3.00002-8; Author:Martin; Document ID:00002; Chapter ID:c0010

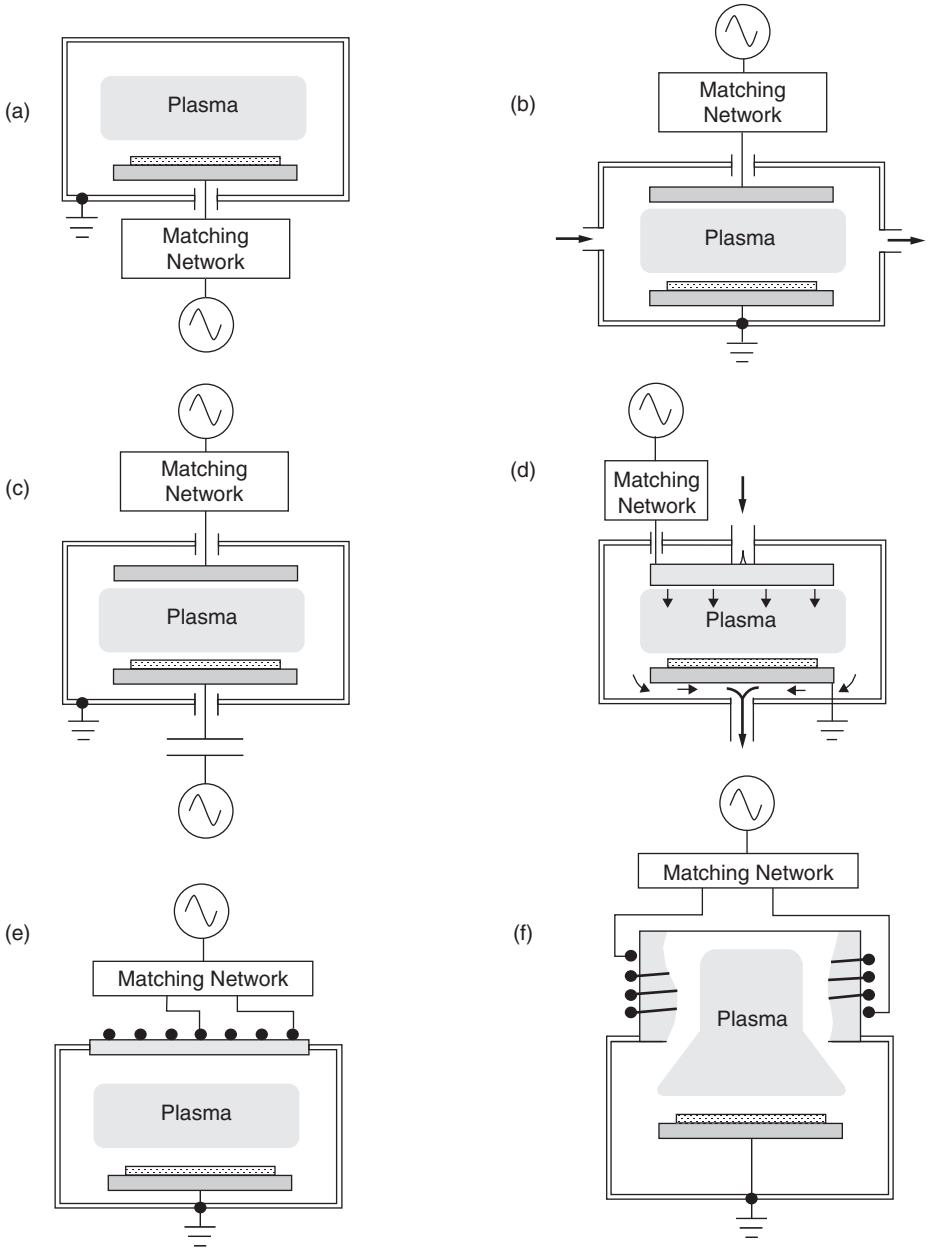


sp0075 **Figure 2.14: Schematic illustrations of apparatus configurations used in materials processing.**

st0095 ### *2.4.2 Plasma Production and Breakdown*

p0445 The degree of ionization in a glow discharge depends on a balance between the rate at which ionization proceeds via electron impact and the rate at which particles are lost by volume

ISBN: 978-0-8155-2031-3; PII: B978-0-8155-2031-3.00002-8; Author:Martin; Document ID:00002; Chapter ID:c0010

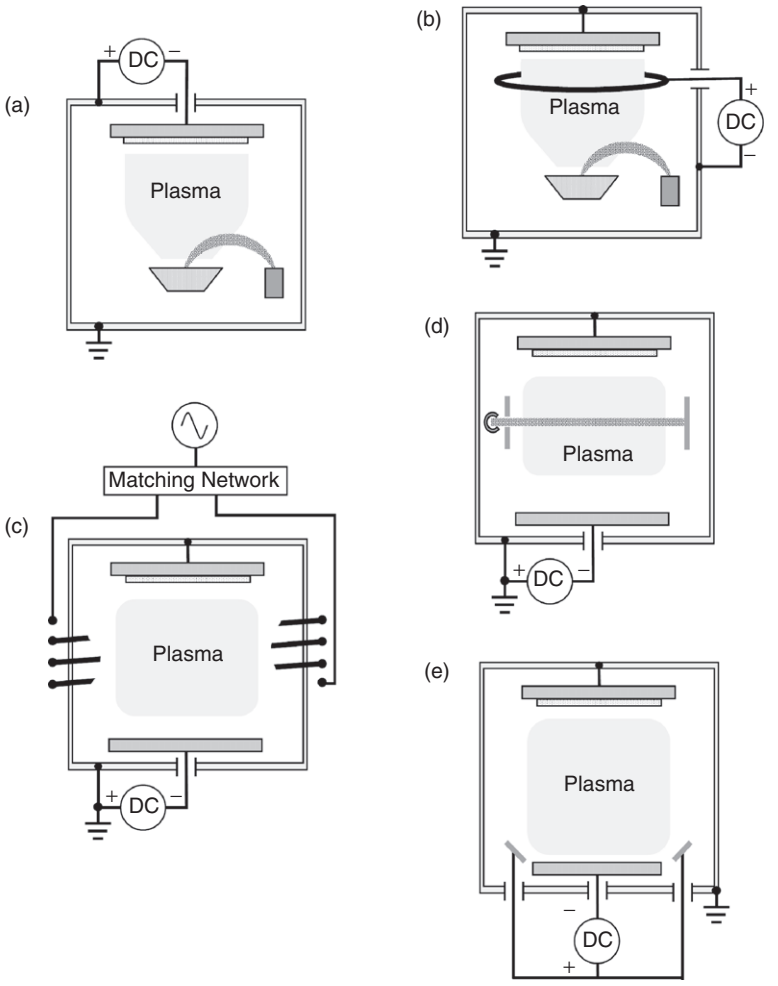


sp0080 **Figure 2.15: Schematic illustrations plasma-assisted PVD apparatus. (a) Ion plating device, (b) activated reactive evaporation device, (c) ICP sputtering device, (d) electron beam generated plasma sputtering device, and (e) cathodic arc device.**

recombination and by passage to the walls of the apparatus. The rate of ionization depends on a relationship of the form (see Eqs. 2.6, 2.8, and 2.15)

$$R_{\mathrm{i}} \propto N n_{\mathrm{e}} \sqrt{\sigma_{\mathrm{ion}}(E)} \tag{2.44}$$

Thus, the rate of ionization depends on the type of gas (through the ionization cross-section $\sigma_{\mathrm{ion}}$), the electric field strength (through the electron energy), and the gas pressure (through the particle density $N$). For most low-pressure configurations, wall losses generally dominate over volume recombination. Accordingly, the occurrence of a breakdown (i.e. the initiation of the

ISBN: 978-0-8155-2031-3; PII: B978-0-8155-2031-3.00002-8; Author:Martin; Document ID:00002; Chapter ID:c0010

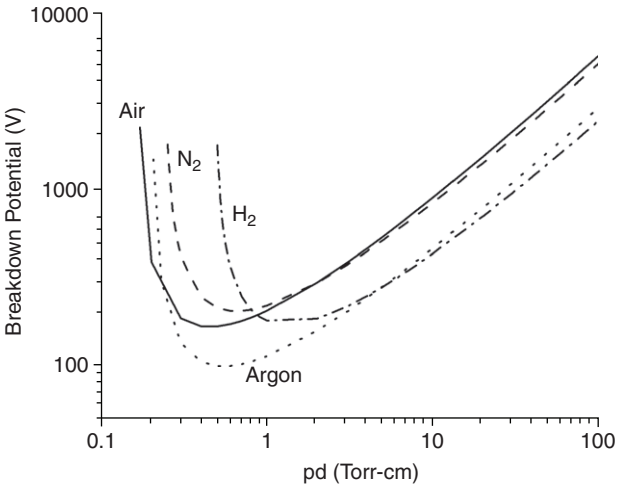


sp0085 **Figure 2.16: Paschen curves for breakdown between parallel, planar electrodes in air, nitrogen, hydrogen, and argon. (Adapted from [48], p. 209.)**

plasma) and the resulting discharge depend on apparatus geometry, gas type and pressure, the electric field strength, and on the surface-to-volume ratio of the plasma. Figure 2.16 shows the interelectrode breakdown voltage as a function of the product of the gas pressure p and the electrode spacing d for plane parallel electrodes in various gases [48]. Such curves are determined experimentally and are known as Paschen curves. Relationships of the same general form apply to the conditions under which a steady-state discharge can be sustained. In such cases, the electrode separation d may be replaced by a characteristic diffusion length for the plasma reactor [18, 49].

p0450 The rise in voltage at the low p-d side in Figure 2.16 occurs because the apparatus is small, or the gas density low, such that electrons are lost to the walls faster than they be created through ionizing collisions. The rise in the required voltage on the right side happens because the electron energy is becoming too low to produce ionization. This can occur at high pressures, because electron collisions with gas atoms become so frequent that the electrons lose energy faster than they can accumulate it, via field acceleration, in order to exceed the ionization potential. It can also occur at a given applied voltage in a very large chamber where local electric fields in the plasma are too weak to deliver sufficient energy to the electrons between collisions. That is, the electric fields are too weak to sustain the plasma over that volume of gas.

p0455 The curves in Figure 2.16 also provide a useful guide for adjusting the operating conditions within a given device in order to produce a plasma discharge. Conversely, the relation provides guidance for the prevention of breakdown on unwanted surfaces. In that case one simply places a grounded shield over the surface to be protected, ensuring that the spacing d between

ISBN: 978-0-8155-2031-3; PII: B978-0-8155-2031-3.00002-8; Author:Martin; Document ID:00002; Chapter ID:c0010

sp0190 **Table 2.3: Typical operating conditions and plasma parameters for low-pressure argon plasmas. The values of $T_e$ and $n_e$ are for the bulk plasma**

| Source | Driving frequency | Power (W) | Pressure (mtorr) | $T_e$ (eV) | $n_e$ ($cm^{-3}$) | Ref. |
|---|---|---|---|---|---|---|
| Helicon | 13.56 MHz | < 1300 | 4–35 | 3–5 | $10^{12}$–$10^{13}$ | [50] |
| ICP RF | 13.56 MHz | 1000 | 4–20 | 2–3 | $2–6 \times 10^{11}$ | [51] |
| CCP RF | 13.56 MHz | 25–50 | 7.6 | 5–2.5 | $0.4–1 \times 10^{11}$ | [52] |
| Magnetron | DC | 100 | 3–15 | 1–3 | $2–10 \times 10^{12}$ | [53] |
| ECR | 2.45 GHz | 200–500 | 0.5–5 | 4–5 | $5 \times 10^{11}$ | [54] |
| Electron beam | Pulsed | 100 | 50 | 1.0 | $3 \times 10^{11}$ | [55] |

the shield and the cathode is small enough that the required breakdown voltage is larger than the voltage used to form and sustain plasma discharge at the operating pressure of interest.

p0460 The above considerations are also important in apparatus scaling. A discharge sustained in a small apparatus must have a high average electron energy to counteract wall losses. Such a discharge, with the same electron density but in a larger apparatus size, will be sustained at a lower average electron energy. This can, in turn, change the active species that are produced. Thus, small-diameter discharge tubes are sometimes used in lasers to elevate the average electron energy to a desired value. Typical discharge electron densities are in the range of $10^8$–$10^{12}$ $cm^{-3}$ with average electron energies of 1–30 eV (as shown in Figure 2.1). A sampling of densities and electron temperatures is shown in Table 2.3 for various plasma sources used in materials processing.

st0100 ### *2.4.3 Cold Cathode Discharges*

p0465 A low-pressure cold cathode discharge is one which is maintained primarily by secondary electrons emitted from the cathode due to bombardment by ions from the plasma. This is in contrast to hot cathodes, where electron emission is primarily thermionic. A classic example of a cold cathode, glow discharge is illustrated in Figure 2.17. Ion-induced secondary electrons are accelerated in the cathode dark space and enter the negative glow, where they are known as primary electrons. Each primary electron must produce a sufficient number of ions to result in the ejection of another secondary electron from the cathode [36]. The secondary electron emission coefficient is typically about 0.1 for low-energy $Ar^+$ ions (a common ion in sputtering plasmas) incident on clean metal surfaces [56]. Thus, primary electrons must produce about ten ion–electron pairs. The coefficient is dependent on incident ion energy and surface conditions. For example, it is larger for some oxidized surfaces but still small enough that each primary electron must produce, or lead to the production of, a plurality of ions [36].

ISBN: 978-0-8155-2031-3; PII: B978-0-8155-2031-3.00002-8; Author:Martin; Document ID:00002; Chapter ID:c0010

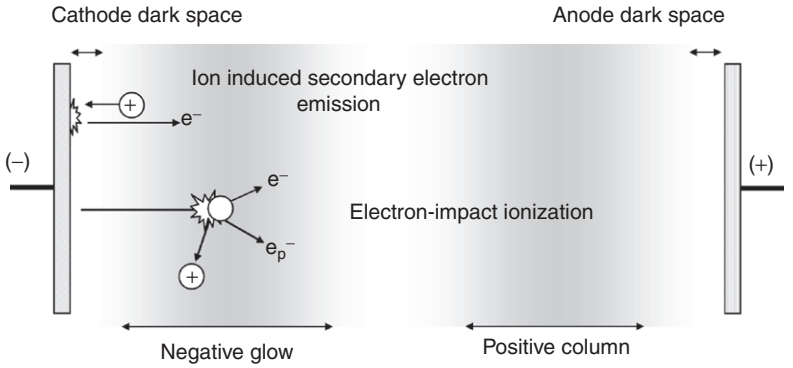


sp0090 **Figure 2.17: Schematic illustration of a simplified cold-cathode discharge. Ion-induced secondary electron emission at the cathode, which leads to ionization in the negative glow, is also shown.**

p0470 The negative glow region of the plasma is where the primary electrons expend their energy, and its extent corresponds to the range of their travel from the cathode [17, 36], where the range depends on both electron energy and gas pressure. The electron energy distribution in the negative glow is multimodal. It consists of primary electrons, reduced-energy primary electrons (primaries that have lost some of their initial energy via collisions), and much larger numbers of low-energy electrons produced during ionization, which are considered part of the plasma electron population. In the classical glow discharge described in most textbooks, a positive column extends from the anode toward the negative glow [11, 21, 23]. In the positive column the electric field is just sufficient to transport the discharge current from the negative glow to the anode and to produce sufficient ionization to compensate for wall losses.

p0475 In planar-diode sources of the type shown in Figures 2.13 and 2.14, the substrate mounting table or anode generally intercepts the negative glow and there is no positive column. From the Paschen relationship discussion (Section 2.4.2), a consequence of this small interelectrode spacing is that the operating pressures are relatively high. For example, reasonable operating conditions for DC planar-diode Ar sputtering discharges are 75 mtorr pressure with a substrate-to-cathode spacing of 4.5 cm, a current density of 1 mA/cm$^2$, and a discharge voltage of 3 kV.

p0480 In order for a cold-cathode discharge to operate effectively at low pressures, it is necessary that the primary electrons be preserved and not lost from the system until they have had a chance to expend enough of their energy in ionization. The hollow cathode geometry shown in Figure 2.18 is effective in this respect because the electrons are trapped by the plasma. Electrons which are accelerated in the cathode dark space and enter the negative glow cannot escape once they have lost an amount of energy about equal to their initial ejection energy (which is only a few eV) [56] since they encounter a sheath with repulsive forces whenever they

ISBN: 978-0-8155-2031-3; PII: B978-0-8155-2031-3.00002-8; Author:Martin; Document ID:00002; Chapter ID:c0010

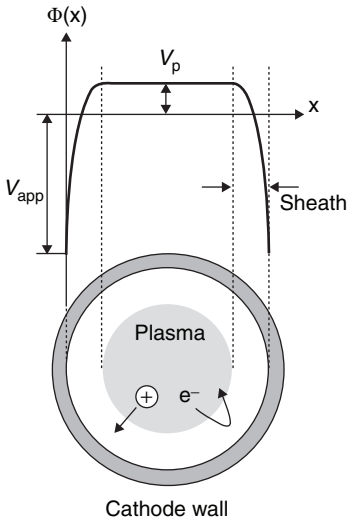


sp0095 **Figure 2.18: Schematic illustration of a hollow cathode discharge (cross-section) along with the potential profile.**

approach the cathode wall. The only losses are out of the ends, and long hollow cathodes with minimized end losses can be operated effectively at low pressures and voltages. For this reason, hollow cathodes are often used as ionization [57] or electron [58] sources.

st0105 ### *2.4.4 Magnetron Discharges*

p0485 Magnetron discharge sources are quite prevalent in sputter deposition applications and will be discussed at the end of this chapter and in greater detail in later chapters. Magnetrons are cold cathode discharge devices in which magnetic fields are used in concert with cathode surfaces to form traps which are so configured that the $E \times B$ electron drift currents can close upon themselves [59]. The cylindrical-post configuration shown in Figure 2.19 provides one example of a magnetron. Primary electrons which leave the cathode rod and enter the plasma find themselves trapped in an annular cavity which is closed on three sides by the cathode surfaces (the hollow cathode effect) and on the fourth side by the magnetic field. The electrons can diffuse across the magnetic field and reach the anode only by making collisions (the process illustrated in Figure 2.7b) and by plasma oscillations (see Section 2.3.3) [44]. Like hollow cathodes, confinement leads to high ionization rates and so cylindrical-post magnetrons are extremely efficient and operate at pressures of less than 1 mtorr with high current densities (10–200 mA/cm$^2$) and low voltages (300–800 V). Planar magnetrons are perhaps the most important devices used in sputter-deposition technology [60]. An example of one is shown in cross-section in Figure 2.20. In this geometry, the magnetic fields confine the plasma above the cathode in annular rings, which produces the well-known erosion profile found in used cathode (target) materials.

ISBN: 978-0-8155-2031-3; PII: B978-0-8155-2031-3.00002-8; Author:Martin; Document ID:00002; Chapter ID:c0010

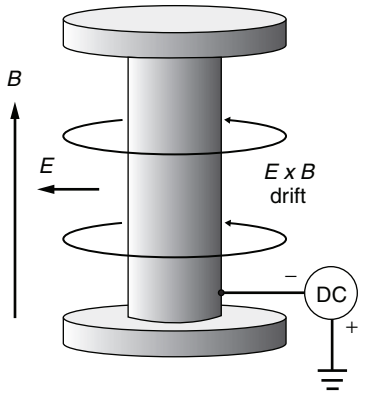


sp0100 **Figure 2.19: Cylindrical-post magnetron sputtering source.**

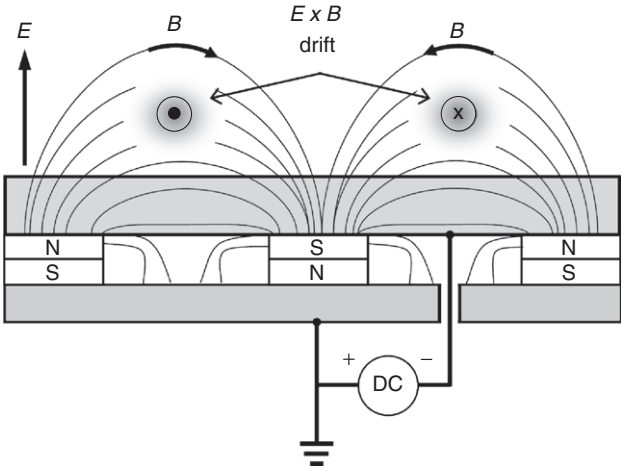


sp0105 **Figure 2.20: Planar magnetron sputtering source. (From [61].)**

p0490 Although the use of DC power is common in magnetrons, RF or pulsed power are also used. High-power impulse magnetron sputtering (HIPIMS) [62], a particular novel approach to the use of magnetrons, uses a short ($\sim 10\,\mu s$) high-voltage pulse delivered to the magnetron surface producing a transient plasma. During peak performance, current densities at the magnetron surface are on the order of $\sim 1\ A/cm^2$ and plasma densities are as high as $10^{13}\ cm^3$. High ion fluxes, comprised of both metal and gas ions, at the substrate surface are useful for certain applications.

st0110 ### *2.4.5 RF Discharges*

p0495 RF-driven planar diode discharge devices of the type shown in Figures 2.13 and 2.14 are used for sputter deposition, plasma-assisted etching, and PACVD. Their application to sputtering is discussed in detail in later chapters.

ISBN: 978-0-8155-2031-3; PII: B978-0-8155-2031-3.00002-8; Author:Martin; Document ID:00002; Chapter ID:c0010

p0500 The operating frequency is generally 13.56 MHz, since this is within the frequency range (10–20 MHz) allocated by the Federal Communications Commission (FCC) for industrial applications. At frequencies above about 1 MHz, only the electrons can follow the temporal variations in applied potential (see Section 2.3). Thus, the plasma can be pictured as an electron gas that moves back and forth at the applied frequency in a sea of relatively stationary ions. As the electron cloud approaches one electrode, it uncovers ions at the other electrode to form a positive ion sheath. This sheath takes up nearly the entire voltage as in the DC case. The ions are accelerated by this voltage and bombard the electrodes.

p0505 The RF discharge can be further understood by examining the electrode current flow. These discharges are often capacitive in nature, because of external capacitance which is placed in the electrical circuit and because one or both electrode surfaces are generally non-conducting, made of either semiconducting or insulating materials. Such plasma sources are thus called capacitively coupled plasmas (CCPs). Since the total ion and electron charge flow to a given electrode during an RF cycle must balance to zero, a DC self-bias ($V_{sb}$) that is negative with respect to the plasma potential develops on any surface that is capacitively coupled to an RF discharge [63]. The basis for this behavior is illustrated in Figure 2.21, where the current voltage characteristics are shown for an electrode immersed in a plasma. When an RF voltage signal is delivered to the electrodes, much larger currents are drawn when the electrode is positive relative to the floating potential than when it is negative, because of the mobility difference between the electrons and the ions (upper figure). In order to achieve zero net current flow, it is necessary for the DC self-bias to develop such that the average potential is negative relative to the floating potential, as shown in the lower figure. This offset means the electrodes only minimally exceed the floating potential (and become anodes), for short portions of each RF cycle. Most of the time they are cathodes. Because the ions largely respond to the DC self-bias they flow to both electrodes throughout the cycle in quantities that are equal to the time-averaged electron flow.

p0510 RF discharges in planar diodes can be operated at considerably lower pressures than DC discharges. Typical operating pressures are 5–15 mtorr. This is due to two reasons: a reduction in the loss of ionizing electrons and an increase in the volume ionization efficiency. In order to understand this, consider that a fraction of the ionizing electrons will be repelled from the electrode toward which they are accelerated as the cycle changes. Thus wall loses decrease, and electrons remain in the discharge longer to make additional ionizing collisions. In addition, electrons can gain energy from the RF field by making in-phase collisions with gas atoms. That is, if an electron, accelerated in one direction during a given half-cycle, makes an elastic collision in which its direction is reversed, it maintains most of its velocity (due to the large mass mismatch between electrons and ions). If this happens near the end of the cycle, it will again be accelerated during the next half-cycle and thus have gained energy during the complete cycle. As the pressure is increased, collision probability increases and the volume ionization due to electrons accelerated by the oscillating electric field becomes increasingly

ISBN: 978-0-8155-2031-3; PII: B978-0-8155-2031-3.00002-8; Author:Martin; Document ID:00002; Chapter ID:c0010

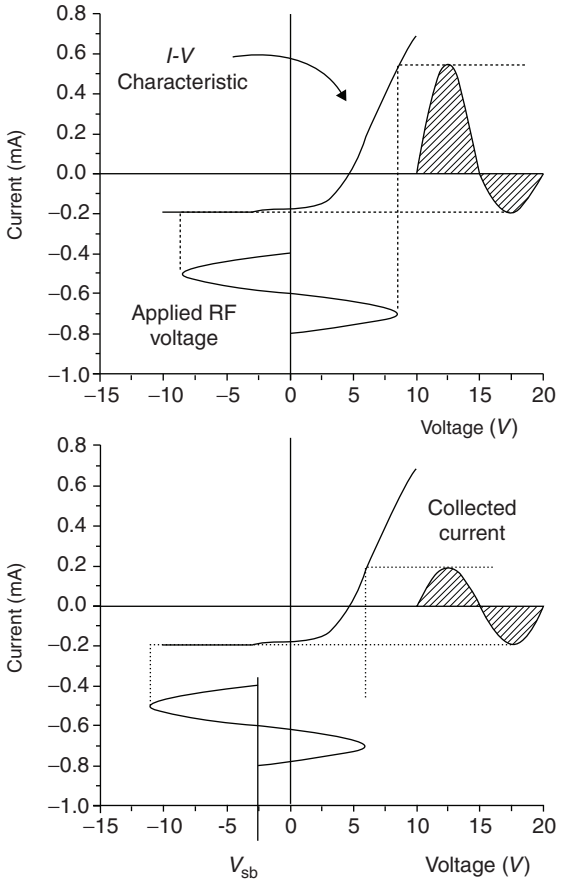


sp0110 **Figure 2.21: Illustration of the formation of a negative bias on a capacitively coupled surface in an RF glow discharge. (Adapted from [63].) The current–voltage (*I–V*) characteristic (similar to a Langmuir probe trace) defines the current collected at an electrode of a given voltage. With the RF voltage applied about zero, the time-averaged collected current will favor electrons. For the time-averaged current to equal zero, the surface to which the RF voltage is applied will adjust to a negative value ($V_{sb}$).**

important. When the planar and cylindrical plasma discharge devices shown in Figure 2.14 are used for plasma-assisted etching, PACVD, and polymerization, the operating pressures are generally high enough that volume-accelerated electrons dominate in producing excitation and ionization. The same is true for high-frequency microwave-driven discharges, such as electron cyclotron resonance (ECR) sources.

p0515 The discussion of RF plasma generation has focused mainly on the electric field to excite the gas. That is, the changing applied electric field permeates the gas to directly accelerate (or decelerate) the plasma electrons. However, RF currents driven through coils will produce an

ISBN: 978-0-8155-2031-3; PII: B978-0-8155-2031-3.00002-8; Author:Martin; Document ID:00002; Chapter ID:c0010

alternating magnetic field, external to the coil, that can induce alternating currents in a gas. Plasma sources that rely on this type of energy transfer are called inductively coupled plasmas (ICPs) and are most common when the geometry is like that shown in Figure 2.13(b). This arrangement is similar to a transformer core, where the gas volume replaces the iron core and so the terms 'transformer coupling' and 'inductive coupling' are used interchangeably. An advantage of ICPs relates to the induced electron currents, which follow circular orbits in planes normal to the device axis. This motion limits the loss of electrons at the chamber walls. Thus, compared to CCPs, where the use of electrodes to deliver power further enhances wall losses, ICPs have plasma densities that are typically an order of magnitude (or more) greater than CCPs.

st0115 ## 2.5 Gas-Phase Plasma Reactions

st0120 ### *2.5.1 Introduction*

p0520 The interaction of charged and neutral particles within the bulk plasma not only sustains the plasma but also defines the chemistry of the plasma, and the production of chemically active species is vital to the production and modification of materials. The complex nature of plasma generation, gas-phase chemistry, and delivery of species to the substrate are illustrated in Figure 2.22.

p0525 Electron bombardment of atoms and molecules can result in dissociation, excitation, and ionization. These inelastic collisional processes (kinetic energy is not conserved) are important

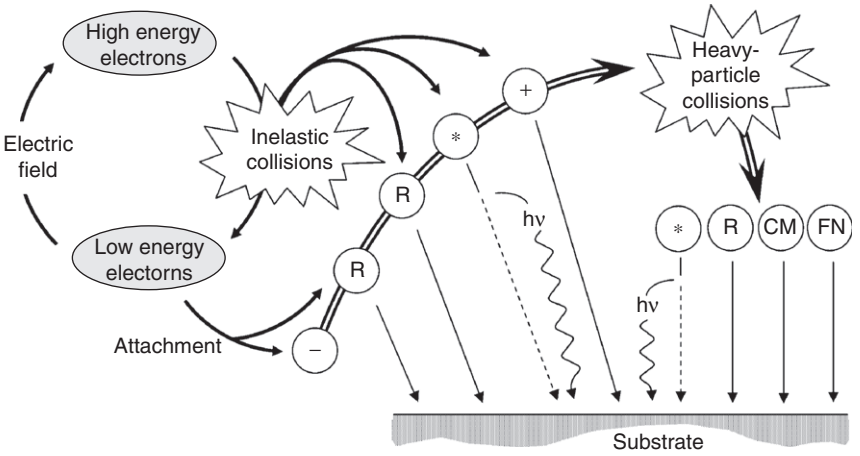


sp0115 **Figure 2.22: Schematic illustration of the generation of active species in a plasma produced in a molecular gas and their delivery to a negatively biased substrate. Included are: negative ions (−), radicals (R), excited species (*), photons (hν), compound molecules (CM), and fast neutrals (FN).**

ISBN: 978-0-8155-2031-3; PII: B978-0-8155-2031-3.00002-8; Author:Martin; Document ID:00002; Chapter ID:c0010

for a number of reasons. Electron ionization processes are obviously important in sustaining the plasma, while excitation and dissociation produce reactive species that are critically important in such processes as reactive sputter deposition, plasma-assisted etching, PACVD, and plasma polymerization. The variety of excited and ionized species, as well as radicals (reactive dissociation products), in a plasma has a much different chemical reactivity than those of the parent gas [64, 65]. For example, although He and Ar atoms are inert, $He^+$ ions with one valence electron are chemically similar to hydrogen, while $Ar^+$ ions can react with $H_2$ molecules to form $ArH^+$ ions [64]. Similarly, $N_2$ is largely inert, but N radicals formed from the dissociation of $N_2$ are reactive and important in the formation of metal-nitride thin films.

st0125 ### *2.5.2 Electron–Atom Interactions*

p0530 As noted, the interaction of energetic electrons with atoms can be either elastic or inelastic. The former is sufficiently understood classically; that is, a collision of two hard spheres in which kinetic energy and momentum is conserved. For inelastic collisions, where kinetic energy is not conserved, the interaction is not sufficiently understood classically. Instead, it is best understood by recognizing that the atom gains an amount of internal energy equal to the loss of electron kinetic energy. This internal energy results in the promotion of an electron to a higher energy level, thereby creating an excited atom. Of course, this transferred energy must be in discrete amounts since the energy levels are quantized. Excited states are limited in their lifetimes and will decay by emitting a photon as the electron falls back to its ground state level. Excited states called metastables, however, can last for very long times and can be significant in low-pressure discharges (see Section 2.5.4). If there is enough energy transferred, the electron can be liberated from the atom producing an ion [66]. For large impacting electron energies, the process could leave the ion in an excited state, the secondary (ejected) electron could have excess kinetic energy, or the impacting electron could retain a large amount of energy. All of these are best described by noting that an electron passing close by an atom does not simply knock an electron to a higher orbit or out of the atom, but produces a perturbation of the atom leading to either excitation or ionization.

p0535 In making plasma calculations, the average energy $W_{ei}$ spent by an electron in creating an electron–ion pair in a given gas or gas mixture is often used. Values of $W_{ei}$ for various atoms and molecules are shown in Table 2.4 along with values for the ionization potential I and first excited states. Typically, $W_{ei}/I \approx 2$–3. It should be noted that $W_{ei}$ is determined using high-energy electrons and the values shown in Table 2.4 are valid for energies above several keV. At low impacting energies more energy is consumed in excitation and elastic collisions, thus more energy is required to produce an ion–electron pair. For plasmas with average electron energies in the range of a few eV, the values of $W_{ei}$ will be larger than those given in Table 2.4 [67].

ISBN: 978-0-8155-2031-3; PII: B978-0-8155-2031-3.00002-8; Author:Martin; Document ID:00002; Chapter ID:c0010

sp0195 **Table 2.4: $W_{ei}$, approximate energy spent to create electron–ion pairs [66], $E_{ion}$, the ionization energy, and $E_m$, the first metastable level**

| Atom or molecule | $W_{ei}$ (eV) | $E_{ion}$ (eV) | $E_m$ (eV) |
|---|---|---|---|
| He | 46 | 24.58 | 19.7 |
| Ne | 37 | 21.56 | 16.6 |
| Ar | 26 | 15.76 | 11.6 |
| Kr | 24 | 14.00 | 9.9 |
| Xe | 22 | 12.13 | 8.3 |
| $H_2$ | 36 | 15.43 | |
| $N_2$ | 36 | 15.59 | |
| NO | 29 | 9.250 | |
| CO | 35 | 14.04 | |
| $O_2$ | 32 | 12.15 | |
| $CO_2$ | 34 | 13.81 | |
| $C_2H_2$ | 28 | 11.40 | |
| $CH_4$ | 29 | 12.99 | |
| $C_2H_4$ | 28 | 10.54 | |
| $C_2H_6$ | 27 | 11.65 | |
| $C_3H_6$ | 27 | 9.73 | |
| $C_3H_8$ | 26 | 11.15 | |
| $C_6H_6$ | 27 | 9.23 | |

st0130 ### 2.5.3 Electron–Molecule Interactions

p0540 The interaction of energetic electrons with molecules differs from interactions with atoms because a molecule has many ways, or degrees of freedom, to absorb electron energy. The types of reactions to consider are listed roughly in terms of the energy threshold (although there is overlap) for a generic molecule:

Attachment: $e + AB \rightarrow AB^-$

Dissociative attachment: $e + AB \rightarrow A + B^-$

Excitation: $e + AB \rightarrow AB^* + e$

Dissociation: $e + AB \rightarrow A + B + e$

Ionization: $e + AB \rightarrow AB^+ + e + e$

Dissociative ionization: $e + AB \rightarrow A^+ + B + e + e$

ISBN: 978-0-8155-2031-3; PII: B978-0-8155-2031-3.00002-8; Author:Martin; Document ID:00002; Chapter ID:c0010

Low-energy electrons can attach to electronegative molecules to form negative ions [68] and since there is an abundance of low-energy electrons in plasmas, negative ions are common in plasmas when the ambient contains electronegative gases such as $CF_4$, $SF_6$, and oxygen [69]. For oxygen, the reactions leading to negative ion formation are [70]:

$$e^- + O_2 \rightarrow O^- + O$$

$$e^- + O_2 + O_2 \rightarrow O_2{}^- + O_2$$

$$e^- + O_2 \rightarrow O^- + O^+ + e^-.$$

The production of $O^-$ from the first reaction has a maximum cross-section of $1 \times 10^{-18}\,cm^2$ at about 6.5 eV, while the three body reaction leading to the production of $O_2{}^-$ has an appreciable rate only when pressures approach 1 torr. Negative ion-positive ion pair production requires electron energies above about twice the ionization energy of $O_2$ and has a cross-section of about $0.3 \times 10^{-18}\,cm^2$.

p0545 The processes of attachment and dissociative attachment convert a fraction, sometimes a significant fraction, of electrons to negative ions. This conversion can have a strong influence on the plasma characteristics given the large mass difference between the negative ions and electrons and can lead to lower conductivity compared to plasmas with little or no negative ion density. In rare cases, negative ions can be the primary negative charge carrier and significantly change the plasma characteristics [71, 72]. In most processing discharges, however, the attachment rate is too low to eliminate the dominance of electrons.

p0550 Electron interactions with molecules produce excitation and ionization via mechanisms essentially identical to those described above for atoms. The primary difference is in the fate of the excitation energy. In atoms, the excitation energy is lost by radiation unless the transitions are quantum-mechanically forbidden (see Section 2.5.4). In molecules, it may result in dissociation of the molecules. Consider the case of $CF_4$, a gas which is commonly used in plasma etching. The threshold for producing excitation is 12.5 eV [73]. The excitation reaction can be written as

$$e^- + CF_4 \rightarrow CF_4{}^* + e^-$$

where the symbol * refers to an excited species. There is evidence that all electronic excitation processes in $CF_4$ produce dissociation [73], wherein the excited states last for a short amount of time and the decay proceeds via dissociation of the molecule. In this two-step excitation–dissociation process, one bond is broken, and the reaction proceeds as

$$CF_4{}^* \rightarrow CF_3 + F$$

ISBN: 978-0-8155-2031-3; PII: B978-0-8155-2031-3.00002-8; Author:Martin; Document ID:00002; Chapter ID:c0010

The primary radicals produced favor F, rather than $CF_2$ and $F_2$ [74]. The active F atoms produced in this way play a very important role in many plasma etching processes.

p0555 Electron impact ionization can result in simple ionization. Such is the case for oxygen, where

$$e^- + O_2 \rightarrow O_2^+ + 2e^- \ (\Delta H = 12.15\,\text{eV})$$

Or the electron impact can result in dissociative ionization reactions of the form

$$e^- + O_2 \rightarrow O + O^+ + 2e^- \ (\Delta H \approx 18\,\text{eV}).$$

The products of such reactions can be long lived in low-pressure plasmas. Gas-phase recombination of atomic constituents of small molecules such as $F_2$, $H_2$, or $O_2$ requires three body collisions to conserve both energy and momentum. At low pressures, the likelihood of such reactions is very small compared to high-pressure gases and so the lifetime for such atoms can be long. For the case of molecular radicals, however, the energy of dissociation can be distributed within a large number of internal degrees of freedom and so, recombination does not require a third body. Thus, the association efficiency is close to unity for simple molecular radicals [45]. One can have, for example,

$$CH_3 + CH_3 \rightarrow C_2H_6$$

The decay of initial reaction products in cascading reactions, with the development of high molecular weight species, is a well-known characteristic of the radiation chemistry of hydrocarbons and halocarbons in both the gas and solid phases [65].

st0135 ### 2.5.4 Metastable Species and Processes

p0560 Metastable states are those excited states that are forbidden by quantum mechanical considerations from undergoing radiative transitions. Atoms or molecules can be excited directly into metastable states by electron impact or can arrive in these states by radiative decay after having been excited into states of higher energy. Atoms or molecules that are excited into electronic states which can decay radiatively have very short lifetimes ($\sim 10^{-9}$ s). However, metastable states can have sufficiently long lifetimes ($\sim 10^{-3}$ s) and, as such, they can carry their stored electronic energy far from their point of origin.

p0565 Metastable states are depopulated when the atoms undergo collisions with surfaces or other particles and may subsequently pass excitation energy to the substrate, target atom or molecule. Energy can be transferred during gas-phase collisions in Penning processes, causing the excitation or ionization of target atoms or molecules of lower ionization potential. Penning reactions are of the form [75]:

$$A^* + Y \rightarrow A + Y^*$$

ISBN: 978-0-8155-2031-3; PII: B978-0-8155-2031-3.00002-8; Author:Martin; Document ID:00002; Chapter ID:c0010

$$A^* + XY \rightarrow A + XY^*$$

$$A^* + Y \rightarrow Y^+ + A + e^-$$

$$A^* + XY \rightarrow XY^+ + A + e^-$$

$$A^* + XY \rightarrow X^+ + Y + A + e^-$$

p0570 Large populations of metastable species can have important effects on the overall discharge characteristics. Gases with large metastable energies such as He, Ne, and Ar are often added to discharges to promote excitation and ionization rates. Also note that when large metastable populations exist in noble gas plasmas, excitation and ionization rates can also increase since excitation and ionization from metastable levels require less electron energy. However, the increase in ionization rates and thus ion current at substrates may not increase the sputtering rates. When lower mass species with large metastable energies (e.g. He) are used, the increased ion currents at substrates may be offset by the fact that lower mass ions will not remove material as effectively as heavy mass ions (e.g. Ar).

st0140 ### *2.5.5 Applications of Volume Reactions*

p0575 Plasma chemistry, the sum of all volume reactions, plays a significant role in applications like PAPVD, PACVD [76], plasma-assisted etching [77], and plasma polymerization [78]. In some cases, the plasma chemistry is unique in that the reactive species are only produced in plasmas. In most, cases however, the advantage of using a plasma is that it can effectively deliver reactive species which promote surface reactions that would otherwise require high substrate temperatures. Examples include the plasma-assisted deposition of silicon nitride ($Si_3N_4$) using discharges produced in a gas mixture of silane ($SiH_4$) and ammonia ($NH_3$) or tetraethoxysilane [$(C_2H_5O)_4Si$] in an oxygen background to grow silicon dioxide ($SiO_2$) films. The plasma chemistry is complicated in both applications, but the important point is that the substrate temperature is typically 300 °C or lower. When the same reactions are carried out by conventional thermal CVD techniques, the substrate temperatures are typically between 800 and 1200 °C [79]. Lower substrate temperatures in PACVD are important in electronic applications where coatings are deposited onto device structures with low thermal budgets and particularly where substrates are sensitive to high surface temperatures, such as polymers.

p0580 A typical electron energy distribution (Figure 2.5) indicates that most electrons are below the ionization energy. Thus, most electron-impact reactions are non-ionizing and, as such, the number of radicals and excited species is quite high in most plasmas. The average electron energies in PACVD processes, for example, are typically between 1 and 10 eV, and the plasma chemistry is dominated by excited species and radicals rather than ions [80]. If the creation of

ISBN: 978-0-8155-2031-3; PII: B978-0-8155-2031-3.00002-8; Author:Martin; Document ID:00002; Chapter ID:c0010

radicals via dissociation of the precursor (donor) gases is critical to a given process, bond energies are an important consideration in the selection of precursors. Consider the example of nitride films, where one of the functions of the plasma during deposition is to provide atomic N in the gas phase since the partial pressure of atomic N required to obtain stoichiometric nitride films is much smaller than that of $N_2$. The dissociation of nitrogen via electron impact is given as

$$e^- + N_2 \rightarrow N + N + e^- \ (\Delta H = 9.83\,\text{eV})$$

Here, an electron energy of at least 9.83 eV is required to obtain N atoms by cleaving the $N_2$ molecule. Alternatively, N atoms can be obtained at lower impact energies through the following step cascade starting with $NH_3$:

$$e^- + NH_3 \rightarrow NH_2 + H + e^- \ (\Delta H = 4.76\,\text{eV})$$

$$e^- + NH_2 \rightarrow NH + H + e^- \ (\Delta H = 3.90\,\text{eV})$$

$$e^- + NH \rightarrow N + H + e^- \ (\Delta H = 3.42\,\text{eV})$$

in which no reaction step requires more than 4.76 eV. For this reason, $NH_3$ can be used in $Si_3N_4$ PACVD. Similarly, nitrous oxide ($N_2O$), rather than oxygen ($O_2$), can be used as a precursor molecule for atoms during PACVD deposition of oxides:

$$e^- + N_2O \rightarrow N_2 + O + e^- \ (\Delta H = 1.73\,\text{eV})$$

$$e^- + O_2 \rightarrow 2O + e^- \ (\Delta H = 4.13\,\text{eV})$$

p0585 Plasma-assisted etching is similar to PACVD, except that a volatile rather than a non-volatile compound is delivered to the substrate. Silicon etching is accomplished by using a discharge to generate reactive F atoms from an inert molecular gas such as $CF_4$. The F atoms cause etching of the Si by forming volatile compounds such as $SiF_4$ on the Si surface.

p0590 Plasma polymerization typically proceeds in a series of steps [81, 82]. For example, high molecular weight species can be formed in a discharge from low molecular weight starting material. These high molecular weight species then condense on substrates, where they are cross-linked by plasma radiation and particle bombardment to form a polymer film. Consider plasma polymerization in acetylene ($C_2H_2$) [83]. The process is initiated by the dissociation of acetylene

$$e^- + C_2H_2 \rightarrow C_2H + H + e^-$$

ISBN: 978-0-8155-2031-3; PII: B978-0-8155-2031-3.00002-8; Author:Martin; Document ID:00002; Chapter ID:c0010

High molecular weight species can then be formed by the reaction of radicals and/or acetylene, such as

$$C_2H_2 + C_2H \rightarrow C_4H_3$$

$$C_2H_2 + C_4H_3 \rightarrow C_4H_4 + \text{products}$$

$$C_2H_2 + C_4H_3 \rightarrow C_6H_5$$

$$C_4H_4 + C_2H \rightarrow C_6H_5 + \text{products}$$

p0595 The gas-phase chemistry can be complex in polymerization processes, involving reactions of electrons and radicals as well as negative and positive ions. Reaction and deposition rates are also dependent on a number of process parameters, including pressure, gas flow, temperature, and delivered RF or DC power.

st0145 ## 2.6 Plasma–Surface Interactions

st0150 ### *2.6.1 Introduction*

p0600 Surfaces in contact with plasmas are bombarded by slow and fast neutrals, electrons, ions, radicals, metastables, complex molecules, and photons, as illustrated in Figure 2.22. The relative importance of each species is largely dependent on the application of interest. Ion bombardment, for example, is of primary interest in sputtering. Electron, ion, and radical impacts are important in reactive ion etching and PAPVD. The interaction of all species is of importance in PACVD, polymer modification, and plasma polymerization. The relative number of ions and electrons which are incident on a surface depends on whether it is biased as a cathode or an anode, or is electrically isolated while the neutral and photon flux is independent of the surface potential. In this section, we briefly discuss some of these interactions and their effects.

st0155 ### *2.6.2 Ion Bombardment*

p0605 Ion bombardment of a surface can liberate neutral and charged species from a surface, as well as change the physical, electrical, and chemical properties of a surface. The momentum exchange associated with ion bombardment can cause surface rearrangement, which can have dramatic effects on the structure and properties of a growing film [46] and is of importance in the processes of ion plating and bias sputtering. Ion-impact can also lead to the ejection (sputtering) of surface atoms. Sputtering of this type is referred to as physical sputtering and will have a strong energy dependence [84]. In addition, ion bombardment can cause a

ISBN: 978-0-8155-2031-3; PII: B978-0-8155-2031-3.00002-8; Author:Martin; Document ID:00002; Chapter ID:c0010

chemical reaction that leads to desorption of volatile surface species in a process called chemical sputtering. Sputtering and desorption are important in the processes of reactive ion etching, sputter cleaning, and deposition. Accordingly, these mechanisms are discussed in later chapters.

p0610 Electrons, positive ions and negative ions can all be ejected as a result of ion impact. Ion-induced charged particle emission often involves more complicated mechanisms than simply momentum (and kinetic energy) exchange, but can lead to similar changes in the surface properties. In the simplest case, electrons can be ejected from a surface as a result of direct ion impact. In this case, ion energies must be high (> 1 keV) given the large mass difference between the ions and electrons [85]. At lower impact energies, however, potential electron emission [86] is an important mechanism and involves electron tunneling out of the metal when the ion is in close proximity to the surface. In a similar process, neutrals leaving the surface, as a result of physical sputtering, can become positive ions when the electron tunnels from the ejected neutral back to the metal [87]. Ion-induced emission of negative ions from a gas-covered surface has been described as an impact-driven surface excitation that can alternatively result in electron emission [88].

p0615 With the exception of ion implantation, the incident ion energies in plasmas processing systems will not exceed a few keV and so it should be assumed that most types of emission mechanism discussed are worth considering, although the relative importance will vary. For the emission of either neutral or charged particles, there is an impact energy dependence to consider. Kinetic processes (i.e. momentum/energy transfer) require energies above some threshold which, generally, will be higher than the energy for the other emission processes mentioned above. The threshold of interest for ion-induced electron emission, for example, is about 1 keV. Above this, emission can be kinetic; below, emission is driven by potential energy differences.

p0620 The magnitude of the incident ion energy will depend on its transit through the sheath that forms adjacent to the surface. There are two general scenarios to consider: one in which ions transit the sheath without collisions and one in which ions collide with gas particles. For collisionless ion transport, the energy of ions bombarding a cathode surface will be about equal to the difference between the cathode potential and the plasma potential, approximately equal to the applied cathode-to-anode potential. This is typical for magnetron sputtering at low pressures (a few mtorr). The current density, bias voltage, sheath thickness, and plasma properties are related by Eqs. (2.38) and (2.39).

p0625 At higher pressures, where ion collisions become important, the bombarding flux consists of both ions and energetic neutrals because of charge exchange collisions (see Figure 2.11). In this case, the average bombardment energies can be considerably less than the potential drop across the sheath. This is illustrated in Figure 2.23 by incident ion energy distributions at a cathode for various pressure regimes (i.e. ratios of sheath length to mean free path). As the mean free path of ions is reduced with respect to the sheath length, an increasing amount of

ISBN: 978-0-8155-2031-3; PII: B978-0-8155-2031-3.00002-8; Author:Martin; Document ID:00002; Chapter ID:c0010

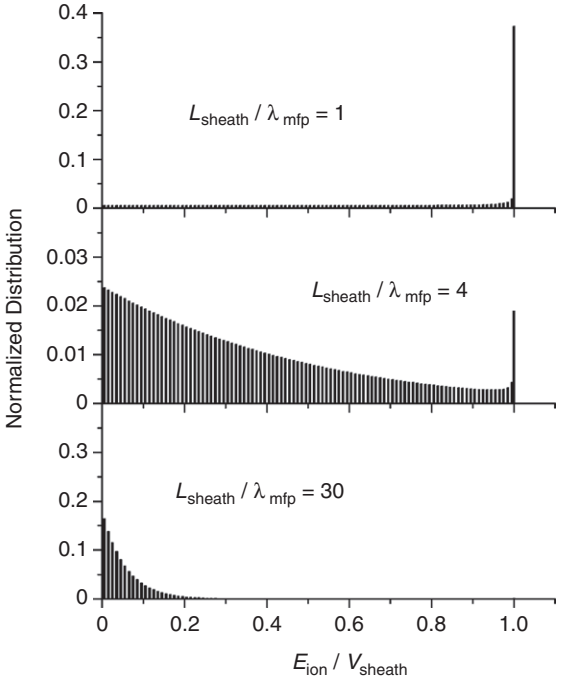


sp0120 **Figure 2.23: Calculated ion-energy distribution histograms showing the effect of charge exchange. (Adapted from [89, 90].) The variable between histograms is the ratio of sheath length $L_{sheath}$ to change exchange mean free path $\lambda_{ex}$. Note scale changes on the vertical axis.**

ions will undergo collision, and reach the cathode with less energy than is available from the sheath potential. Another example is shown in Figure 2.24 where different ion species in the same plasma can be behave very differently [91]. Here, the cross-sections of interest for $N_2^+$ and $N^+$ differ by nearly an order of magnitude. That is, $N_2^+$ ions experience a more collisional sheath than $N^+$ ions. The sheath parameters for the high-pressure case are related to the ion current in Eq. (2.39).

p0630 Ion bombardment can greatly influence the processes involved in the adsorption of molecules onto surfaces and their subsequent reactions. The process of molecular adsorption [92], surface compound formation, and desorption is illustrated in Figure 2.25. The difference between etching and film growth is dependent on the nature of the compounds formed at the surface. When the products are volatile, etching occurs. Any of the steps shown in the figure can be rate limiting. Physical adsorption is due to polarization (van der Waals') bonding. It is a non-activated process and occurs with all gas–surface combinations under appropriate conditions of temperature and pressure. Adsorption energies are typically less than 0.5 eV. Chemisorption involves a rearrangement of the valence electrons of the adsorbed and surface atoms to form a chemical bond. The process has an activation energy and has a high degree of

ISBN: 978-0-8155-2031-3; PII: B978-0-8155-2031-3.00002-8; Author:Martin; Document ID:00002; Chapter ID:c0010

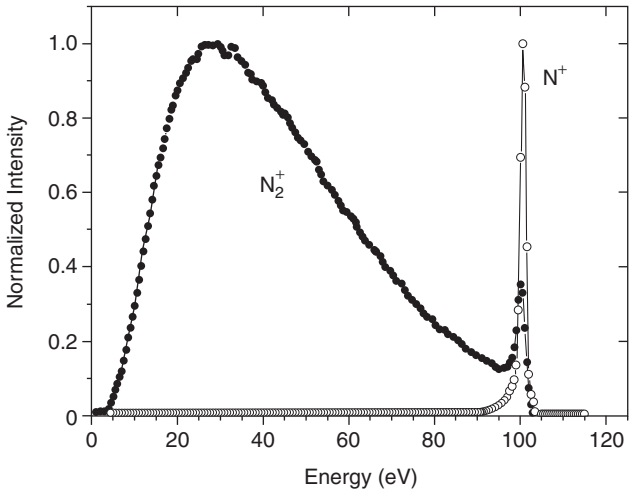


sp0125 **Figure 2.24: $N_2^+$ and $N^+$ ion energy distributions at an electrode adjacent to a 100 V sheath. (From [91]. The plasma was produced in 160 mtorr of $N_2$ and Ar (12%).**

specificity between gas–surface combinations. Typical chemisorption energies are between 1 and 10 eV. Molecules may be chemisorbed in their molecular state or may dissociate into atoms. The latter case is known as dissociative chemisorption and is generally a precursor to compound formation, which is also an activated process. Various types of chemisorption bond sites can exist on a solid surface and so both molecular and dissociative chemisorption can occur simultaneously on the same surface. Ion bombardment can influence these processes in a number of ways. First, it can cause adsorbed molecules to dissociate, thereby overcoming the activation energy for this process. Ion bombardment can also create surface defect sites which have a reduced activation energy for chemisorption or for the formation of a solid compound.

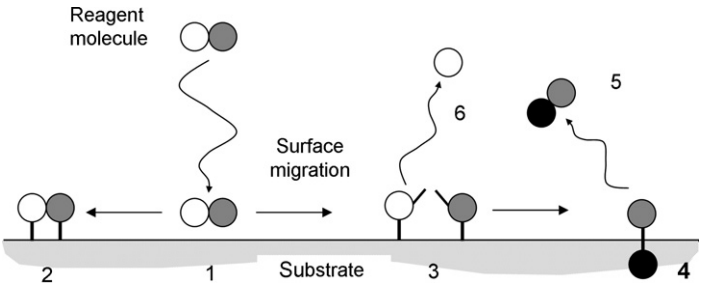


sp0130 **Figure 2.25: Schematic representation of surface adsorption, migration and compound formation during processing. Processes indicated are (1) physisorption, (2) chemisorption, (3) dissociative chemisorption, (4) volatile compound formation and (5) desorption, and (6) desorption of non-reactive species.**

ISBN: 978-0-8155-2031-3; PII: B978-0-8155-2031-3.00002-8; Author:Martin; Document ID:00002; Chapter ID:c0010

Lastly, ion bombardment can remove (by sputtering) foreign species which may inhibit chemisorption of preferred species.

p0635 Molecular ions can break apart upon impacting a surface and their fragments can participate in surface processes. For example, collisionally induced dissociative chemisorption of ions during reactive magnetron sputter deposition has been shown to play a major role in controlling the dynamics of film growth. During homoepitaxial growth of TiN(001) in mixtures of argon and nitrogen, for example, increasing the $N_2$ fraction from 10% to 100% increases the steady-state N coverage $\theta_N$, which, in turn, increases the rate-limiting surface diffusion activation barrier $E_s$ from 1.1 to 1.4 eV over the temperature range 500–865 °C [93, 94]. Corresponding *ab initio* density functional theory calculations [93–96] show that $TiN_x$ ($x = 0, 1, 2, 3$) admolecules are the primary diffusing species. For pure nitrogen, $TiN_2$ and/or $TiN_3$ are the rate-limiting diffusing species, while reducing the nitrogen concentration to 10% increases the coverage of Ti and TiN adspecies at the expense of $TiN_2$ and $TiN_3$, leading to higher surface diffusivities (lower $E_s$) and the observed transition in nucleation kinetics. The reduction in $N_2$ not only reduces the neutral flux but also decreases the $N_2^+$ ion flux to the surface, thereby reducing the amount of N available for heavy nitride compound formation.

p0640 A similar mechanism can be used to control the evolution of preferred orientation in polycrystalline TiN [95, 97] and TaN [98] films deposited at low temperatures on amorphous substrates. Layers deposited in pure $N_2$, but under conditions of very little $N_2^+$ ion irradiation, exhibit approximately equal probabilities of (001) and (111) island nucleation. However, the layers grow with a columnar grain structure which evolves toward (111) preferred ordination in a kinetically limited process with increasing film thickness. The (111) columns gradually overgrow (001) columns owing to the higher chemical potential on high-diffusivity (001) surfaces [i.e. diffusing adspecies have a higher probability of becoming trapped on low-diffusivity (111) grains]. However, dramatically increasing the $N_2^+$ ion flux to the growing films changes the preferred orientation in favor of (001) columns. Since there is no substantial change in $\theta_N$, and (111) grains are always fully N terminated in a strongly reactive environment, collision-induced dissociation of $N_2^+$ ions preferentially increases the steady state N coverage on (001) grains, thereby decreasing the chemical potential, and thus the diffusivity on (001) surfaces.

p0645 Low-energy ion irradiation during film deposition can have dramatic effects on the microstructure and microchemistry, and hence physical properties, of as-deposited layers, as discussed in detail in [46]. Specifically, low-energy ion fluxes have been used to modify film microstructure in the following ways: densification and increased oxidation resistance of optical films; minimization or elimination of columnar microstructure in microelectronic metallization layers; altering the state of stress, average grain size, and preferred orientation; increased film/substrate adhesion; enhanced conformal coverage; controlled magnetic anisotropy in recording layers; and 'low-temperature' epitaxy.

ISBN: 978-0-8155-2031-3; PII: B978-0-8155-2031-3.00002-8; Author:Martin; Document ID:00002; Chapter ID:c0010

p0650 Low-energy ion irradiation is often used during thin-film growth to controllably alter the composition of as-deposited layers. Examples include preferential sputtering from the growing film during deposition of alloys [99–102], enhanced reactive gas incorporation during deposition of compounds [103–106], and increased dopant incorporation probabilities combined with better control of dopant depth distributions [107, 108]. Here again, ion bombardment can result in potentially deleterious effects, depending on experimental design, such as rare-gas incorporation in sputter-deposited films [109–112]. Mechanisms associated with accelerated-particle–film interactions leading to changes in incorporation probabilities range from purely physical effects such as implantation and recoil processes to irradiation-assisted chemistry.

p0655 Most films in the above-mentioned application areas are deposited in the presence of a plasma, by either bias sputter deposition, PAPVD, or PACVD. Since the plasma–surface interface is complex, experiments to isolate ion irradiation effects are often carried out using ion beams. One example is illustrated in Figure 2.26, showing experimental and calculated (Monte Carlo simulations) densities of vapor-deposited $CeO_2$ films grown at ambient temperature while under $O^+$ ion beam irradiation. The experiments were carried out as a function of ion energy $E$, for an ion-to-vapor flux ratio of $J_i/J_v$ of unity [113]. The film density initially increased with increasing ion energy; due primarily to ion implantation, recoil implantation (driving surface atoms into the bulk) and, to a lesser extent, sputtering of weakly bound species. However, at

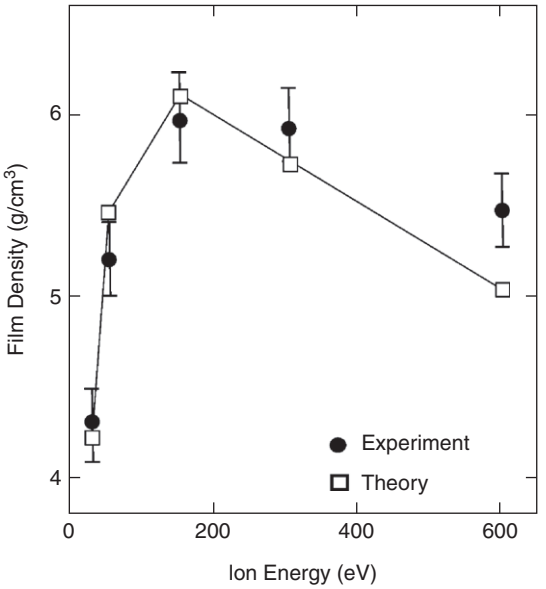


sp0135 **Figure 2.26: Experimental and theoretical values of the density of $CeO_2$ films deposited by simultaneous evaporation of Ce in $O_2$ and $O^+$ ion beam irradiation as a function of ion energy E. The bulk density of $CeO_2$ is 8.1 g/cm$^3$. (From [113].)**

ISBN: 978-0-8155-2031-3; PII: B978-0-8155-2031-3.00002-8; Author:Martin; Document ID:00002; Chapter ID:c0010

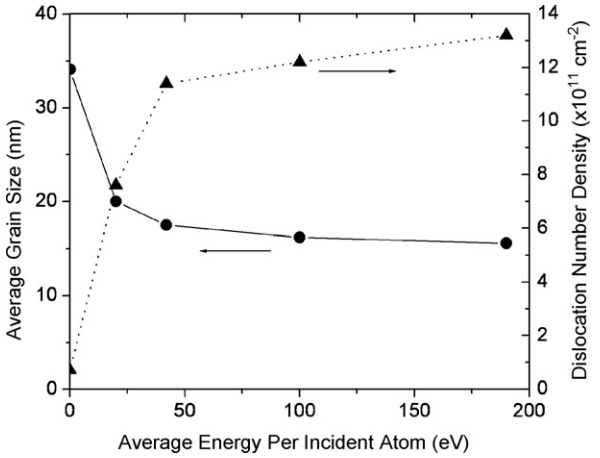


sp0140 **Figure 2.27: The average grain size and dislocation number density in Ag films deposited at room temperature as a function of the average energy per deposited atom. (From [114].)**

high ion energies, an increasing fraction of the ion energy was lost deeper in the lattice leaving vacancies which could not be filled by the above processes The optimum ion energy for densification, which depends on the masses of the collision partners, was approximately 200 eV in this case.

p0660 In other ion beam experiments, it was found that while ion irradiation is useful for increasing the density and modifying the microstructure of films deposited at low temperatures, other irradiation-induced effects that are not beneficial, such as increased defect densities occurring simultaneously. This is shown in Figure 2.27 from the work of Huang et al. [114], who studied the effects of Ar ion bombardment during the growth of Ag films at room temperature using a dual ion beam apparatus. They found that the grain size decreased while the dislocation number density increased with increasing average irradiation energy per deposited Ag atom. At elevated growth temperatures, however, low-energy ion irradiation can have the opposite effect and actually reduce residual defect densities in as-deposited films [115, 116]. Work on damage production and sputter cleaning of substrate surfaces prior to epitaxial growth [117–120] suggests that low-energy ion irradiation-induced damage can be continuously annealed out at elevated temperatures. Yu [120] used low-energy electron diffraction (LEED) to show that the temperature required to maintain a Si(111)7 $\times$ 7 surface reconstruction during $Ne^+$ ion irradiation decreased from $\approx$ 450 to 150 °C as the ion energy was decreased from 500 to 80 eV.

p0665 Low-pressure discharges and plasmas have been used to modify surface chemistry and promote adhesion with vacuum-deposited metal overlayers on polymers. X-ray photoelectron spectroscopy (XPS) studies of the effects of $O_2$ plasma treatments on acrylonitrile butadiene styrene (ABS), polypropylene [121], and polystyrene [122] surfaces showed the formation of

ISBN: 978-0-8155-2031-3; PII: B978-0-8155-2031-3.00002-8; Author:Martin; Document ID:00002; Chapter ID:c0010

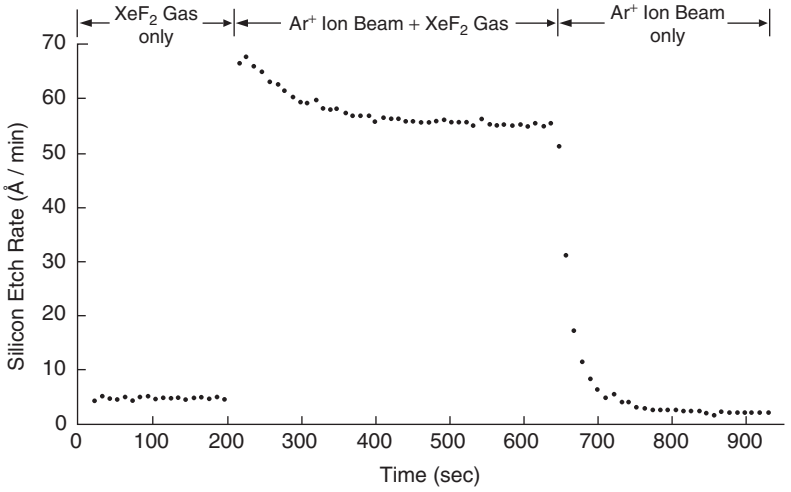


sp0145 **Figure 2.28: The results of ion beam experiments designed to investigate ion-stimulated etching of and Si in $XeF_2$. (From [126].)**

both single and double C–O bonds. The incorporation of oxygen leads to stronger metal overlayer adhesion [123] through the formation of oxygen bridge bonds between C and metal atoms. Ion beam experiments [124] obtained similar increases in metal overlayer adhesion for Ti on polyethylene using an $Ar^+$ ion bombardment pretreatment to remove low molecular weight impurities, promote cross-linking, and allow the formation of a carbidic Ti–C interfacial layer as observed in XPS. Both $Ar^+$ ion irradiation and $O_2$ plasma pretreatments also increased the adhesion of Ti on polydimethylsiloxane (a silicone rubber) owing to the formation of Ti–C and Ti–O bonds [125].

p0670 Reactive ion etching technology also relies heavily on ion-irradiation induced effects for both stimulating chemical reaction channels and increasing the anisotropy of the etch profile. An example of the former is shown in Figure 2.28, illustrating results for $Ar^+$ ion-assisted F/Si chemistry. $XeF_2$ undergoes dissociative chemisorption on Si, forming the compound $SiF_4$ [74, 127], which is volatile at room temperature. The etch rate is limited by the $XeF_2$ flow. However, the Si etch rate increased by an order of magnitude when the Si surface was simultaneously bombarded by 450 eV $Ar^+$ ions. In this case, $Ar^+$ ion irradiation greatly increases the etch rate by promoting dissociative chemisorption. In the absence of $XeF_2$, the etch rate collapses to near zero.

st0160 ### *2.6.3 Electron Bombardment*

p0675 As previously noted, the time-averaged flux of positively and negatively charged species to surfaces exposed to a plasma is comparable. However, since the plasma potential is usually

ISBN: 978-0-8155-2031-3; PII: B978-0-8155-2031-3.00002-8; Author:Martin; Document ID:00002; Chapter ID:c0010

more positive than any surface it is in contact with, electrons are typically decelerated as they leave the plasma. Thus, electrons will impact adjacent surface at relatively low energies compared to the ions. Nonetheless, electron irradiation can cause surface heating and promote chemical changes.

p0680 Electron irradiation is a primary source of substrate heating during film deposition by DC and RF diode sputtering [128, 129]. Energetic electron, as well as photon, irradiation of ionically bonded substrates has also been shown to strongly affect film nucleation kinetics through the creation of charged surface vacancies which act as preferential adsorption sites [130–133]. Reduced epitaxial temperatures, for a given set of deposition conditions, have been reported for many film–substrate combinations, including Si and Ge on NaCl [134] and PbTe on $CaF_2$ [132].

p0685 Unlike the more massive ions, momentum exchange phenomena are not important until electron energies are very large. That is, physical sputtering of surface species is not possible at low electron energies, given the large mass difference between electrons and atoms and molecules. However, electron-stimulated desorption (ESD) [135] by low-energy electrons can cause the ejection of neutral or charged particles from the surface. In this process, low-energy electrons cause an excitation in surface species, allowing them to overcome the potential barrier (adsorption energy) such that the atom or molecule is ejected from the surface as a neutral, positive ion [136, 137], or negative ion [138]. Electron-induced surface excitations can give rise to changes in surface chemistry during film growth through, for example, excitation and ionization of adsorbed or surface molecules into states leading to dissociation, bond rearrangement, or desorption. In the treatment of polymers [139], electron radiation can create surface radicals, which leads to polymerization. It is important to recognize that this process is limited to the surface and will not influence the bulk properties directly, since electron penetration is limited owing to the low incident energies.

p0690 An example of electron-stimulated surface chemistry during plasma etching is shown in Figure 2.29. $XeF_2$ dissociatively chemisorbs on $SiO_2$, but etching does not occur because of a high activation barrier for the reaction channel leading to the formation of $SiF_4$, Electron bombardment alone has been observed to remove O from the surface of $SiO_2$ and produce elemental Si [140, 141], but it does not cause etching. However, when $SiO_2$ is subjected to electron bombardment in the presence of $XeF_2$, etching occurs at relatively high rates, $\approx$200 Å/min in the example given in Figure 2.29 [126].

st0165 ### *2.6.4 Photon Interactions*

p0695 Plasmas emission will typically include the soft X-ray, ultraviolet, visible and near-infrared regions, which extend from about 50 nm up to 1000 nm, corresponding to energies ranging from about 25 eV to 1 eV. This range of energies is adequate to initiate excitation that leads to

ISBN: 978-0-8155-2031-3; PII: B978-0-8155-2031-3.00002-8; Author:Martin; Document ID:00002; Chapter ID:c0010

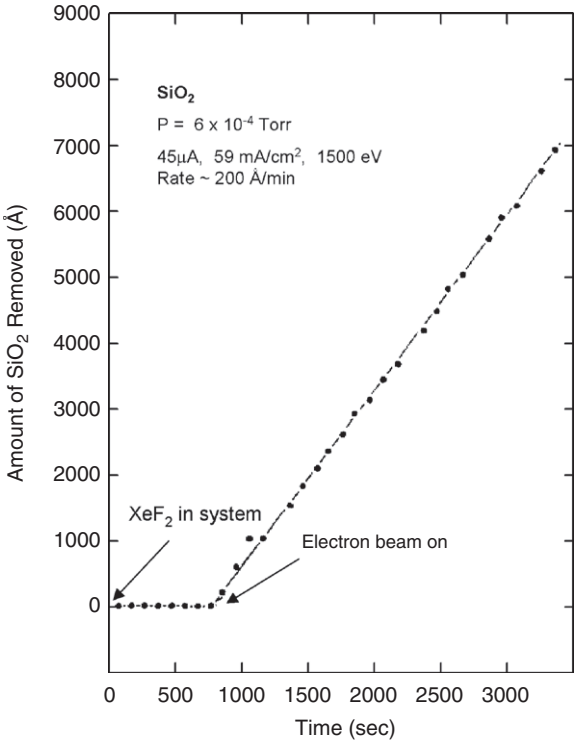


sp0150 **Figure 2.29: The results of beam experiments designed to investigate electron-stimulated etching of $SiO_2$ in $XeF_2$. (From [126].)**

dissociation, bond rearrangement, or desorption as described above for electrons. In fact, the mechanisms for ESD are similar for photon-stimulated desorption [142, 143], and both fall into the more broadly described grouping, desorption induced by electronic transitions (DIET) [144]. The emission of neutral [145], positive ions [142], and negative ions [146] from gas-covered surfaces has been observed. Photon-induced radical formation in plasma-treated polymers has also been identified as a mechanism that can lead to polymerization [139]. It is important to recognize that unlike particle impact at low energies, photons can penetrate or even pass through certain materials. In the case of polymers, photons can promote chemical changes below the surface [147].

st0170 ### *2.6.5 Summary of Surface Reactions*

p0700 The plasma–surface interaction is a complex one. There are many different reactions to consider and each of these will depend on the operating parameters of a given plasma processing application. Particle and photon flux will vary strongly with background gas,

ISBN: 978-0-8155-2031-3; PII: B978-0-8155-2031-3.00002-8; Author:Martin; Document ID:00002; Chapter ID:c0010

operating pressure, and applied power. The secondary emission yield or chemical changes at the surface will, in turn, depend on the material, conditions of the surface, and surface bias.

p0705 Most of the mechanisms described above are studied in well-controlled experiments. Thus, the extrapolation of these reactions to plasma processing environments is, at best, an estimate. Moreover, the combined ion, electron, and photon flux can provide a certain synergy that may or may not be well understood. For these reasons, many plasma–surface reactions remain less than well understood even though the overall results are well known for a given plasma source and operating condition.

## st0175 2.7 An Example: Magnetron Discharge for Deposition

p0710 The volumetric or gas-phase features of plasmas combined with plasma–surface interactions discussed in this chapter are important in understanding the operation of planar magnetrons for deposition applications. Many of these are exemplified by Figures 2.30 and 2.31, which show results from reactive magnetron sputter deposition of $TiN_x$ $(0 < x < 1)$ as a function of $Ar/N_2$ gas composition (ranging from pure Ar to pure $N_2$) [148]. The total pressure prior to initiating

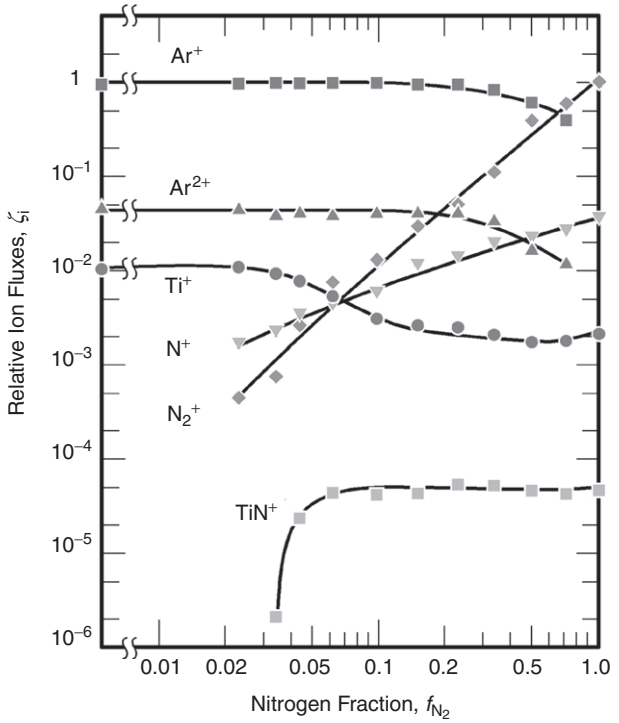


sp0155 **Figure 2.30: Relative ion fluxes measured during reactive magnetron sputter deposition of $TiN_x$ in $Ar/N_2$ mixtures as a function of relative nitrogen concentration. (From [148].)**

ISBN: 978-0-8155-2031-3; PII: B978-0-8155-2031-3.00002-8; Author:Martin; Document ID:00002; Chapter ID:c0010

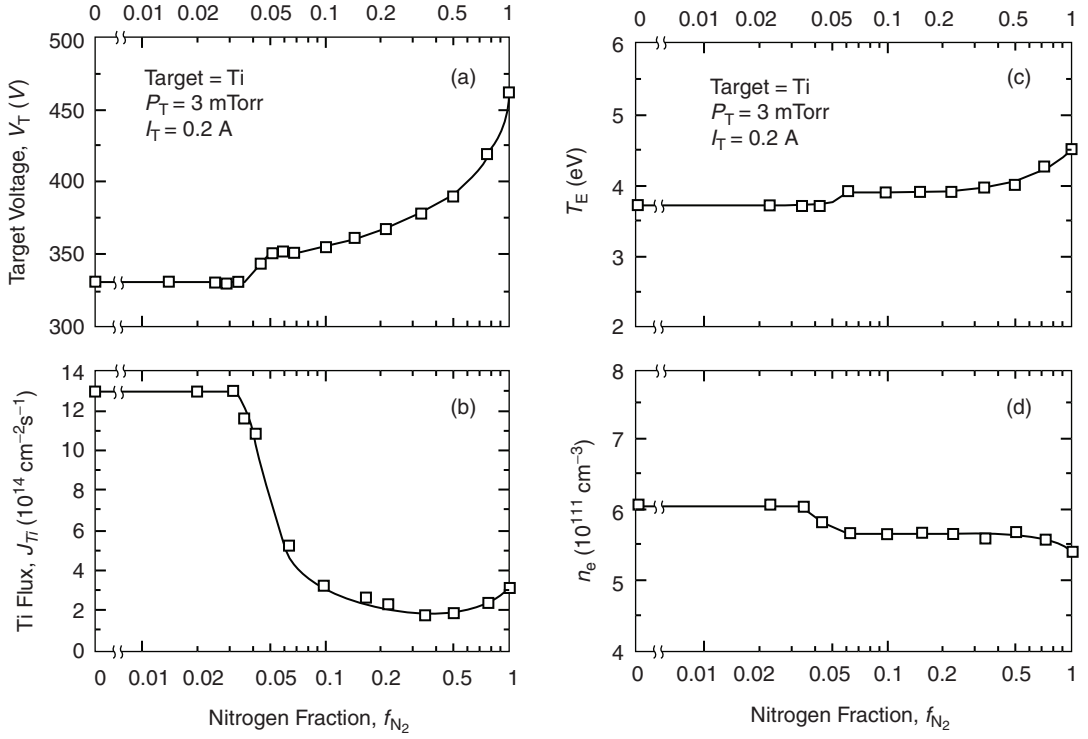


sp0160 **Figure 2.31: (a) Target voltage, (b) titanium flux, (c) electron temperature, and (d) plasma density measured as a function of relative nitrogen concentration during reactive magnetron sputter deposition of $TiN_x$ in $Ar/N_2$ mixtures. (From [148].)**

the discharge is maintained at 3 mtorr (0.4 Pa), for which the charge exchange mean free path is more than ten times the anode (substrate) sheath width. Figure 2.30 shows the relative fluxes of ions incident at the negatively biased substrate plane, determined using a combination of high-resolution mass and energy resolved spectrometry. The results of Figure 2.31 were determined using Langmuir probes, and measurements of film composition and deposition rate.

p0715 Comparing the incident-ion results from Figure 2.30, 'simple' plasmas composed of pure gases already yield some interesting results. In pure Ar, the dominant ion incident at the substrate is $Ar^+$, followed by $Ar^{2+}$ at approximately 4%, and $Ti^+$ ions at less than 1%. The $Ti^+$ ions are sputtered atoms ionized in the plasma (the flux of $Ti^+$ ions sputter ejected from the target is more than an order of magnitude less) [148, 149]. For these three species, the ionization energies are as follows:

$$e^- + Ar \rightarrow Ar^+ + 2e^- \ (\Delta H = 15.76\,eV)$$

$$e^- + Ar \rightarrow Ar^{2+} + 3e^- \ (\Delta H = 27.53\,eV)$$

$$e^- + Ti \rightarrow Ti^+ + 2e^- \ (\Delta H = 6.83\,eV)$$

ISBN: 978-0-8155-2031-3; PII: B978-0-8155-2031-3.00002-8; Author:Martin; Document ID:00002; Chapter ID:c0010

p0720 As noted earlier in this chapter, only the electrons in the high-energy part of the distribution have sufficient energy to ionize gaseous species. It follows that $Ar^{2+}$ ions, with a much higher ionization energy, are present at relatively low concentrations and that they are primarily formed in the narrow cathode sheath by inelastic collisions with fast electrons. The flux of $Ti^+$ ions is low (even though the Ti ionization potential is small) owing to the low partial pressure of Ti atoms compared to Ar.

p0725 In pure $N_2$ discharges, $N_2^+$ comprises approximately 96% of the total ion flux, while $N^+$ and $Ti^+$ account for only 3.5% and 0.2%, respectively. Even though the electron density and energy distribution has changed, the fact that $J(N_2^+) \gg J(N^+)$ is due primarily to the large difference in electron-impact ionization energies:

$$e^- + N_2 \rightarrow N_2^+ + 2e^- \ (\Delta H = 15.5\,\text{eV})$$

$$e^- + N_2 \rightarrow N^+ + N + 2e^- \ (\Delta H = 24.4\,\text{eV}).$$

p0730 The $Ti^+$ ion flux is significantly reduced from its value in Ar and $TiN^+$ ions are also observed. In pure nitrogen, the target surface is fully nitrided (or 'poisoned') and the effect of this is to dramatically decrease the sputtered neutral Ti atom flux $J(Ti)$ (Figure 2.31b) since the sputtering yield of titanium nitride is much less than that of pure titanium. There is a small, but measurable, flux of $TiN^+$ ions arising from sputtered molecules ionized in the plasma. In addition, the secondary electron yield of titanium nitride is lower than that of Ti, resulting in an increase in the target voltage $V_t$ (Figure 2.31a), since the magnetron is operated in constant current mode, which gives rise to an increase in the average electron temperature from 3.7 to 3.9 eV (Figure 2.31c).

p0735 For the discharges produced in $Ar/N_2$ mixtures, the addition of only $\sim 3.5\%$ $N_2$ ($f(N_2) = 0.035$) already leads to a small flux of molecular $TiN^+$ ions, indicating that even at this low $N_2$ gas-phase concentration, a steady-state coverage of chemisorbed N has accumulated on the target surface which is being sputtered at a relatively high rate. The decrease in the $Ti^+$ ion flux with increasing $f_{N_2}$ is primarily reflecting the reduction in the Ti sputter rate, which occurs in concert with the appearance of $TiN^+$ ions, a decrease in $J(Ti)$, an increase in target voltage $V_t$, and a drop in the secondary electron yield and plasma density $n_e$ (Figure 2.31d). A further small increase in $f(N_2)$ from 0.035 to $\sim 0.060$ results in $J(TiN^+)$, $V_t$, and $J(Ti)$ reaching saturation, a signature of complete nitridation of the target surface. Note that even at $f(N_2) = 0.3$, far past the point of saturation nitridation, $Ar^+$ remains the dominant ion, accounting for about 90% of the total ion flux at the substrate.

p0740 For $Ar/N_2$ mixtures with $f_{N_2} < 0.06$, Figure 2.30 shows that $J(N^+) > J(N_2^+)$, which is contrary to what might be expected from the above discussion. However, in Ar-rich plasmas, $N^+$ ions can be formed by a two-step process in which accelerated $Ar^+$ ions, fast neutrals, and

ISBN: 978-0-8155-2031-3; PII: B978-0-8155-2031-3.00002-8; Author:Martin; Document ID:00002; Chapter ID:c0010

long-lived Ar* metastables collisionally dissociate $N_2$ molecules to N atoms which can then be ionized by electron impact.

p0745 The ionized fraction of sputtered Ti remains relatively constant at $J(Ti^+)/J(Ti) \sim 7 \pm 2 \times 10^{-3}$, irrespective of Ar/$N_2$ gas composition. The small value of the ratio shows that Ti ions contribute little to film growth kinetics. Moreover, from the viewpoint of plasma chemistry, the fact that $J(Ti^+)/J(Ti)$ does not change significantly with $f(N_2)$ indicates that Penning ionization, via collisions with Ar* metastable species, does not play a dominant role in forming metal ions during reactive magnetron sputtering. In contrast to RF discharges, where Penning ionization provides a major contribution to target atom ionization in the gas phase [150], electron impact ionization dominates during DC magnetron sputtering owing to the lower operating pressures and the relatively high electron currents which characterize these devices.

p0750 Achieving high deposition rates (maximum when the target surface is pure metal) while depositing nearly stoichiometric compound films in a reactive gas can prove challenging. For example, it is extremely difficult to operate in the narrow $f(N_2)$ range 0.035–0.060, over which the target surface changes from essentially pure metal to pure nitride, when using a mass flow controller as a closed-loop feedback element. There are two issues here. First, a mass flow controller requires mechanical motion (change in orifice size), which is slow. Second, small perturbations can quickly drive the target to become fully poisoned. A slight increase in N concentration on the target leads to an additional decrease in sputtered Ti flux $J(Ti)$, which leads, in turn, to an increase in the extant $N_2$ partial pressure since the primary mechanism for nitrogen loss from the plasma is chemisorption by freshly deposited metal (sputter-deposited Ti acts as an internal sorption pump). The increased $N_2$ pressure further increases the N coverage on the target, and so on in an uncontrolled avalanche effect as the target rapidly becomes fully nitrided and the film deposition rate reaches a minimum. The solution is to use $N_2$ partial pressure, not the flow rate, as the feedback signal [151].

## st0180 2.8 Summary

p0755 In this chapter, we surveyed fundamental aspects of plasmas as they relate to materials processing, particularly deposition and surface modification. This includes the basics of gas-phase interactions, discharge physics, and plasma–surface interactions. It should be clear that plasmas provide an environment not easily attained with other processing approaches. Within the plasma, electrons are able to produce reactive radicals and excited species from otherwise inert gases. At the surface, energetic charged particles bombard the growing film. For the electrons, their kinetic energies are a few electron volts; for the ions, incident energies can be tens of electron volts. In terms of temperature, 1 eV is equivalent to 11,604 K or roughly 40 times room temperature. This might not be a unique property if it were not for the fact that the background gas and adjacent surface are *not* in thermal equilibrium with the plasma species; both the gas and surfaces can be maintained at room temperature. This enables the

ISBN: 978-0-8155-2031-3; PII: B978-0-8155-2031-3.00002-8; Author:Martin; Document ID:00002; Chapter ID:c0010

modification of substrates and production of films at low gas and surface temperatures, which is advantageous for several substrate, gas, and film combinations.

p0760 The delivery of large fluxes of energetic ions to adjacent surfaces is beneficial in deposition applications. The ability to deliver a uniform flux over large areas is important in terms of material utilization and in industrial applications where throughput is of considerable importance. Moreover, most of the ion energy is deposited within a few monolayers of the surface, which is useful when sputtering high- or low-melting point and multicomponent material.

p0765 The production of plasma and plasma-based systems for materials processing is flexible. As outlined, there are many approaches to plasma production and each method has its advantages in terms of plasma and system characteristics. Over the years, several interesting developments have emerged in various processing communities, such as the development of hybrid systems that employ multiple plasma sources and an expansion of operating parameters. Examples include a number of interesting approaches to PAPVD, high-pressure plasma processing techniques in the hope of reducing capital and processing costs associated with maintaining a vacuum, and the use of microdischarges for processing on a very small scale.

p0770 Given the many unique characteristics of plasmas, it is not surprising that plasma-based systems are common to a wide range of applications. The development of new plasma-based processing systems has driven the evolution of materials and vice versa. It is reasonable to expect this close relationship to continue and so an understanding of the basic physics and chemistry of plasmas is vital.

## st0185 Appendix 2.1

p0775 Système International (SI) units are not always the units used in plasma physics and we have adopted the more commonly used units throughout this chapter. The following constants, conversions, and formulae are useful:

p0780 • Unified atomic mass unit: $u = 1.66 \times 10^{-27}$ kg

p0785 • Atomic mass number: $A$ = (number of protons and neutrons) $\approx$ atomic weight ($A_r$)

p0790 • Electron mass: $m_e = 9.11 \times 10^{-31}$ kg = (1/1836) u

p0795 • Heavy particle mass: $M = A \times 1.67 \times 10^{-27}$ kg

p0800 • Electron volt (eV): one electron volt is the energy gained by a particle with unit charge which is accelerated in an electric field produced by a potential difference of one volt ($1\ \text{eV} = 1.602 \times 10^{-19}$ J = 11,604 K)

p0805 • Electron plasma frequency: $f\,(\text{Hz}) = 9000\ (n_e\ (\text{cm}^{-3}))^{1/2}$

ISBN: 978-0-8155-2031-3; PII: B978-0-8155-2031-3.00002-8; Author:Martin; Document ID:00002; Chapter ID:c0010

p0810 • Electron Debye length: $\lambda_d$ (cm) = 740 ($T_e$ (eV)/$n_e$ (cm$^{-3}$))$^{1/2}$

p0815 • Average electron speed at electron temperature: $v$(cm/s) = $5.95 \times 10^7$ ($T_e$(eV))$^{1/2}$

p0820 • Average gas velocity at gas temperature: $v$(cm/s) = $1.58 \times 10^4$ ($T$(K)/$M$(u))$^{1/2}$

p0825 • Boltzmann constant (k): k = $1.38 \times 10^{-23}$ J/K = $8.62 \times 10^{-5}$ eV/K

p0830 • Ideal gas law: $PV = kT$

p0835 • Room temperature: 20 °C = 293 K (for convenience 300 K is often used)

p0840 • Gas density ($N$): at 1 torr and 300 K (27 °C), $N = 3.2 \times 10^{16}$ particles/cm$^3$

p0845 • Atmospheric pressure at sea level: 760 orr

p0850 • 1 torr = 133.3 Pa = 1 mmHg = 1.316 mbar.

## Acknowledgements

p0180 S.G. Walton gratefully acknowledges the support of the Office of Naval Research and his colleagues at the Naval Research Laboratory, Dr R.F. Fernsler and NRC/NRL postdoctoral research associates, Dr E.H. Lock and Dr M. Baraket for their helpful comments and discussions. J.E. Greene gratefully acknowledges the support of the Office of Naval Research and the Materials Science Division of the Department of Energy over the course of several years.

## References

bib0010 [1] J.A. Thornton, J.E. Greene, in: R.F. Bunshah (Ed.), Deposition Technologies for Films and Coatings, 2nd ed., Noyes Publications, Westwood, NJ, 1994, p. 55.
bib0015 [2] R. Rejoub, B.G. Lindsay, R.F. Stebbings, Phys. Rev. A 65 (2002) 042713.
bib0020 [3] N.J. Mason, W.R. Newell, J. Phys. B 20 (1987) 1357.
bib0025 [4] J. Bretagne, G. Callede, M. Legentil, V. Puech, J. Phys. D 19 (1986) 761.
bib0030 [5] A. Chutjian, D.C. Cartwright, Phys. Rev. A 23 (1981) 2178.
bib0035 [6] M. Hayashi, National Technical Information Document No. N82-18007. Copies may be obtained from the National Technical Information Service, Springfield, VA 22161.
bib0040 [7] Y. Itikawa, J. Phys. Chem. Ref. Data 38(1) (2009) 1.
bib0045 [8] D. Rapp, D.D. Briglia, J. Chem. Phys. 43(5) (1965) 1480.
bib0050 [9] I. Iga, M.V.V.S. Rao, S.K. Srivastava, J.C. Nogueira, Z. Phys. D Atoms, Molecules and Clusters 24 (1992) 111.
bib0055 [10] A.V. Phelps, J. Phys. Chem. Ref. Data 20(3) (1991) 557.
bib0060 [11] J.O. Hirschfelder, C.F. Curtiss, R.B. Bird, Molecular Theory of Gases and Liquids, Wiley, New York, 1954, p. 523.
bib0065 [12] L.S. Frost, A.V. Phelps, Phys. Rev. 127 (1962) 1621.
bib0070 [13] R.D. White, K.F. Ness, R.E. Robson, Appl. Surf. Sci. 192 (2002) 26.
bib0075 [14] R.E. Robson, R.D. White, Z.Lj. Petrovic, Rev. Mod. Phys. 77 (2005) 1303.

ISBN: 978-0-8155-2031-3; PII: B978-0-8155-2031-3.00002-8; Author:Martin; Document ID:00002; Chapter ID:c0010

bib0080 [15] G.W. Sutton, A. Sherman, Engineering Magnetohydro-dynamics, McGraw-Hill, New York, 1965.
bib0085 [16] D.D. Pappas, A.A. Bujanda, J.A. Orlicki, R.E. Jensen, Surf. Coat. Technol. 203 (2008) 830.
bib0090 [17] J.D. Cobine, Gaseous Conductors, Dover, New York, 1958.
bib0095 [18] R.F. Baddour, R.S. Timmins (Eds.), The Applications of Plasmas to Chemical Processing, MIT Press, Cambridge, MA, 1967.
bib0100 [19] J.A. Thornton, J. Vac. Sci. Technol. 15 (1978) 188.
bib0105 [20] H.R. Griem, Plasma Spectroscopy, McGraw-Hill, New York, 1964, p. 129.
bib0110 [21] D. ter Haar, Elements of Statistical Mechanics, Holt, Rinehart and Winston, New York, 1960, p. 381.
bib0115 [22] H. Akashi, S. Samukawa, N. Takahashi, T. Sasaki, Jpn. J. Appl. Phys. 36 (1997) 877.
bib0120 [23] B. Ramamurthi, D.J. Economu, I.D. Kaganovich, Plasma Source Sci. Tech. 12 (2003) 302.
bib0125 [24] V. Godyak, Phys. of Plasma 12 (2005) 055501.
bib0130 [25] S.-H. Seo, J.-H. In, H.-Y. Change, Plasma Source Sci. Tech. 13 (2004) 409.
bib0135 [26] N. Herskowitz, in: D.A. Glocker, S. Ismath Shah (Eds.), Handbook of Thin Film Process Technology, Institute of Physics Publishing, Bristol, 1995.
bib0140 [27] R.F. Fernsler, Plasma Sources Sci. Technol. 18 (2009) 014012.
bib0145 [28] D.J. Rose, M. Clar Jr, Plasmas and Controlled Fusion, MIT-Wiley, New York, 1961, p. 80.
bib0150 [29] F.F. Chen, Introduction to Plasma Physics, Plenum Press, New York, 1974.
bib0155 [30] J.D. Huba, NRL Plasma Formulary (Revised), Naval Research Laboratory, Washington, DC, 1998.
bib0160 [31] L. Spitzer Jr, Physics of Fully Ionized Gases, Interscience, New York, 1956.
bib0165 [32] S.M. Rossnagel, in: J.L. Vossen, W. Kern (Eds.), Thin Film Processes II, Academic Press, New York, 1991, p. 42.
bib0170 [33] J.L. Delcroix, Introduction to the Theory of Ionized Gases, Interscience, New York, 1960, p. 128.
bib0175 [34] S. Chapman, T.G. Cowling, The Mathematical Theory of Non Uniform Gases, Cambridge University Press, Cambridge, 1960, p. 90.
bib0180 [35] Y. Ikezoe, S. Matsuoka, M. Takebe, A. Viggiano, Gas Phase Ion–Molecule Reaction Rates Through 1986, Ion Reaction Research Group of the Mass Spectroscopy Society of Japan, Distributed by Maruzen Co., Tokyo, Japan, 1989.
bib0185 [36] H.W. Ellis, R.Y. Pai, E.W. McDaniel, E.A. Mason, L.A. Viehland, Atomic Data and Nuc. Data Tables 17 (1976) 177.
bib0190 [37] S.C. Brown, Basic Data of Plasma Physics, MIT Press, Cambridge, MA, 1959.
bib0195 [38] E.W. McDaniel, The Mobility, Diffusion of Ions in Gases, Wiley, New York, 1973, p. 132.
bib0200 [39] M.H. Mittleman, in: F.H. Clauser (Ed.), Plasma Dynamics, Addison-Wesley, New York, 1960, p. 54.
bib0205 [40] F.F. Chen, in: R.H. Huddlestone, S.L. Leonard (Eds.), Plasma Diagnostic Techniques, Academic Press, New York, 1965, p. 113.
bib0210 [41] D. Bohm, E.H.S. Burhop, H.S.W. Massey, in: A. Guthrie, R.K. Wakerling (Eds.), The Characteristics of Electrical Discharges in Magnetic Fields, McGraw-Hili, New York, 1949, p. 13.
bib0215 [42] M.A. Lieberman, A.J. Lichtenberg, Principles of Plasma Discharges and Materials Processing, Wiley-Interscience, New York, 1994.
bib0220 [43] S. Glasstone, R.H. Louberg, Controlled Thermonuclear Reactions, Van Nostrand, New York, 1960, p. 459.
bib0225 [44] J.A. Thornton, J. Vac. Sci. Technol. 15 (1978) 171.
bib0230 [45] F.K. McTaggart, Plasma Chemistry in Electrical Discharges, Elsevier, New York, 1967.
bib0235 [46] J.E. Greene, S.A. Barnett, J.E. Sundgren, A. Rockett, Ion Beam Assisted Film Growth, Elsevier, Amsterdam, 1988, p. 101.
bib0240 [47] R.F. Bunshah, A.C. Raghuram, J. Vac. Sci. Technol. 9 (1972) 1385.
bib0245 [48] A. Fridman, L.A. Kennedy, Plasma Physics and Engineering, Taylor and Francis, New York, 2004.
bib0250 [49] S.C. Brown, A.D. MacDonald, Phys. Rev. 76 (1949) 1629.
bib0255 [50] R.T.S. Chen, N. Hershkowitz, Phys. Rev. Lett. 80(21) (1998) 4677.
bib0260 [51] K. Takenaka, Y. Setsuhara, K. Nishisaka, A. Ebe, S. Sugiura, K. Takahashi, K. Ono, Jpn. J. Appl. Phys. 45 (10B) (2006) 8046.
bib0265 [52] M. Nisha, K.J. Saji, R.S. Ajimsha, N.V. Joshy, M.K. Jayaraj, J. Appl. Phys. 99 (2006) 033304.


ISBN: 978-0-8155-2031-3; PII: B978-0-8155-2031-3.00002-8; Author:Martin; Document ID:00002; Chapter ID:c0010

bib0270 [53] P. Sigurjonsson, J.T. Gudmundsson, J. Phys.: Conference Series 100 (2008) 062018.
bib0275 [54] D. Leonhardt, C.R. Eddy Jr, V.A. Shamamian, R.F. Fernsler, J.E. Butler, J. Appl. Phys. 83(6) (1998) 2971.
bib0280 [55] S.G. Walton, D. Leonhardt, R.F. Fernsler, IEEE Trans. Plasma Sci. 33(2) (2005) 0093–3813.
bib0285 [56] E.S. McDaniel, Collision Phenomena in Ionized Gases, Chap. 13, Wiley, New York, 1964.
bib0290 [57] D.G. Williams, J. Vac. Sci. Technol. 11 (1974) 374.
bib0295 [58] S.G. Walton, C. Muratore, D. Leonhardt, R.F. Fernsler, D.D. Blackwell, R.A. Meger, Surf. Coat. Technol. 186(1–2) (2004) 40.
bib0300 [59] J.A. Thornton, A.S. Penfold, in: J.L. Vossen, W. Kern (Eds.), Thin Film Processes, Academic Press, New York, 1978.
bib0305 [60] R. Parsons, in: J.L. Vossen, W. Kern (Eds.), Thin Film Processes II, Academic Press, New York, 1991, p. 178.
bib0310 [61] M. Baraket, Elaboration et caractérisation de revêtements nano-structurés à base de nitrure de chrome par pulvérisation cathodique magnétron en condition réactive – propriétés mécaniques et tribologiques, Thesis, Université de Technologie de Belfort-Montbéliard, 2008.
bib0315 [62] A.P. Ehiasarian, R. New, W.-D. Munz, L. Hultman, U. Helmersson, V. Kouznetsov, Vacuum 65 (2002) 147.
bib0320 [63] H.S. Butler, G.S. Kino, Phys. Fluids 6 (1963) 1346.
bib0325 [64] W.F. Libby, J. Vac. Sci. Technol. 16 (1979) 414.
bib0330 [65] G.M. Burnett, A.M. North (Eds.), Transfer and Storage of Energy by Molecules, Wiley-Interscience, New York, 1969.
bib0335 [66] L.G. Christophourou, Atomic and Molecular Radiation Physics, Wiley-Interscience, New York, 1971, p. 6.
bib0340 [67] M.A. Lieberman, A.J. Lichtenberg, Principles of Plasma Discharges and Materials Processing, Wiley-Interscience, New York, 1994, p. 81.
bib0345 [68] L.G. Christophorou, D.L. McCorckle, A.A. Christodoulides, in: L.G. Christophorou (Ed.), Electron–Molecule Interactions and their Applications , Vol. 1, Academic Press, New York, 1984.
bib0350 [69] E. Stoffles, W.W. Stoffels, D. Vender, M. Haverlag, G.M.W. Krosen, F.J. DeHoog, Contrib. Plasma Phys. 35 (1995) 331.
bib0355 [70] Y. Itikawa, A. Ichimura, K. Onda, K. Sakimoto, K. Takayanagi, Y. Hatano, M. Hayashi, H. Nishimura, S. Tsurubuchi, J. Phys. Chem. 18(1) (1989) 23.
bib0360 [71] S.G. Walton, D. Leonhardt, R.F. Fernsler, R.A. Meger, Appl. Phys. Lett. 81(6) (2002) 987.
bib0365 [72] S.G. Walton, R.F. Fernsler, Plasma Source Sci. Technol. 18 (2009) 022001.
bib0370 [73] H.F. Winters, J.W. Coburn, E.J. Kay, Appl. Phys. 48 (1978) 4973.
bib0375 [74] J.W. Coburn, H.F. Winters, J. Vac. Sci. Technol. 16 (1979) 392.
bib0380 [75] E.E. Muschlitz Jr, Science 159 (1968) 599.
bib0385 [76] J.R. Holiahan, R.S. Rosier, in: J.L. Vossen, W. Kern (Eds.), Thin Film Processes, Academic Press, New York, 1978, p. 335.
bib0390 [77] C.M. Melliar-Smith, C.J. Mogab, ibid., p. 497.
bib0395 [78] H. Yasuda, ibid., p. 361.
bib0400 [79] W. Kern, V.S. Ban, ibid., p. 257.
bib0405 [80] T.B. Gorczyca, B. Gorowitz, in: N.G. Einspruch, D.M. Brown (Eds.), VLSI Electronics: Microstructure Science, Academic Press, New York, 1984.
bib0410 [81] H. Kobayashi, A.T. Bell, M. Shen, Macromolecules 7 (1974) 277.
bib0415 [82] J.M. Tibbitt, R. Jensen, A.T. Bell, M. Shen, Macromolecules 10 (1977) 647.
bib0420 [83] S. Stoykov, C. Eggs, U. Kortshagen, J. Phys. D 34 (2001) 2160–2173.
bib0425 [84] H.H. Anderson, H.L. Bay, in: R. Behrisch (Ed.), Sputtering by Particle Bombardment I, Springer, Berlin, 1981, p. 145.
bib0430 [85] E.V. Alonso, M.A. Alurralde, R.A. Baragiola, Surf. Sci. 166 (1986) L155.
bib0435 [86] H.D. Hagstrum, Phys. Rev. 96 (1954) 325, Phys. Rev. 96 (1954) 336.
bib0440 [87] M.L. Yu, N.D. Lang, Nuc. Inst. Meth. B 14 (1986) 403.

ISBN: 978-0-8155-2031-3; PII: B978-0-8155-2031-3.00002-8; Author:Martin; Document ID:00002; Chapter ID:c0010

bib0445 [88] J.C. Tucek, S.G. Walton, R.L. Champion, Phys Rev B 53(21) (1996) 14127.
bib0445 J.C. Tucek, R.L. Champion, in: Surf. Sci. 382 (1997) 137.
bib0450 [89] W.D. Davis, T.A. Vanderslice, Phys. Rev. 131 (1963) 219.
bib0455 [90] C.V. Budtz-Jørgensen, J. Bøttiger, P. Kringhøj, Vacuum 56 (2000) 9.
bib0460 [91] C. Muratore, S.G. Walton, D. Leonhardt, R.F. Fernsler, D.D. Blackwell, R.A. Meger, J. Vac. Sci. Technol. A 22(4) (2004) 1530.
bib0465 [92] J.R. Anderson (Ed.), Chemisorption and Reactions on Metallic Films, Academic Press, New York, 1971.
bib0470 [93] M.A. Wall, D.G. Cahill, I. Petrov, D. Gall, J.E. Greene, Phys. Rev. B 70 (2004) 035413.
bib0475 [94] M.A. Wall, D.G. Cahill, I. Petrov, D. Gall, J.E. Greene, Surf. Sci. 581 (2005) L122.
bib0480 [95] D. Gall, S. Kodambaka, M.A. Wall, I. Petrov, J.E. Greene, J. Appl. Phys. 93 (2003) 9086.
bib0485 [96] S. Kodambaka, S.V. Khare, I. Petrov, J.E. Greene, Surf. Sci. Rep. 60 (2006) 55.
bib0490 [97] I. Petrov, P.B. Barna, L. Hultman, J.E. Greene, J. Vac. Sci. Technol. 21 (2003) S117.
bib0495 [98] C.-S. Shin, D. Gall, Y.-W. Kim, N. Hellgren, I. Petrov, J.E. Greene, J. Appl. Phys. 92 (2002) 5084.
bib0500 [99] H.F. Winters, D.L. Ramondi, D.E. Horne, J. Appl. Phys. 40 (1969) 2996.
bib0505 [100] M.L. Tarng, G.K. Wehner, J. Appl. Phys. 42 (1971) 2449.
bib0510 [101] J.J. Cuomo, R.J. Gambino, J. Vac. Sci. Technol. 12 (1975) 79.
bib0515 [102] J.L. Zilko, J.E. Greene, J. Appl. Phys. 51 (1980) 1549.
bib0520 [103] M.J. Brett, R.R. Parsons, Can. J. Phys. 63 (1985) 819.
bib0525 [104] S. Shimizu, T. Tsukakoshi, S. Komiya, Y. Makita, Y. GaAs, Y. Related Compounds, Inst. Phys. Conf. Series 79 (1985) 91.
bib0530 [105] J.M.E. Harper, J.J. Cuomo, H.T.G. Hentzell, J. Appl. Phys. 58 (1985) 550.
bib0535 [106] J.E. Sundgren, B.O. Johansson, A. Rockett, S.A. Barnett, J.E. Greene, Physics and Chemistry of Hard Coatings, American Inst. Phys. Series Conf. Proc. 149 (1986) 95.
bib0540 [107] M.A. Hasan, J. Knall, S.A. Barnett, J.E. Sundgren, L.C. Markert, A. Rockett, J.E. Greene, J. Appl. Phys. 65 (1989) 172.
bib0545 [108] P. Fons, N. Hirashita, L.C. Markert, Y.W. Kim, J.E. Greene, W.X. Ni, J. Knall, G.V. Hansson, J.E. Sundgren, Appl. Phys. Lett. 53 (1988) 1732.
bib0550 [109] H.F. Winters, E. Kay, J. Appl. Phys. 38 (1967) 2928.
bib0555 [110] A. Pan, J.E. Greene, Thin Solid Films 78 (1981) 25.
bib0560 [111] D.W. Hoffman, J.A. Thornton, J. Vac. Sci. Technol. 20 (1982) 355.
bib0565 [112] L. Hultman, L.C. Markert, J.E. Sundgren, J.E. Greene, Appl. Phys. Lett. 53 (1988) 1175.
bib0570 [113] K.H. Muller, Appl. Phys. A 40 (1986) 209.
bib0575 [114] T.C. Huang, G. Lim, F. Parmiagiani, E. Kay, J. Vac. Sci. Technol. A 3 (1985) 2161.
bib0580 [115] L. Hultman, U. Helmersson, S.A. Barnett, J.E. Sundgren, J.E. Greene, J. Appl. Phys. 61 (1987) 552.
bib0585 [116] L. Hultman, S.A. Barnett, J.E. Sundgren, J.E. Greene, J. Cryst. Growth 92 (1988) 639.
bib0590 [117] R. Ronsille, R. Boch, G.L. Destefanis, J.L. Tissot, Appl. Phys. Lett. 44 (1984) 679.
bib0595 [118] J.H. Comfort, L.M. Gaverick, R. Reif, J. Appl. Phys. 62 (1987) 3388.
bib0600 [119] L.M. Gaverick, J.H. Comfort, T.R. Uyeh, R. Reif, F.A. Baiocchi, H.S.J. Luttman, J. Appl. Phys. 62 (1987) 3398.
bib0605 [120] M.L. Yu, Appl. Phys. Lett. 40 (1982) 986.
bib0610 [121] J.M. Burkstrand, J. Vac. Sci. Technol. 15 (1978) 223.
bib0615 [122] J.M. Burkstrand, Appl. Phys. Lett. 33 (1978) 387.
bib0620 [123] D. Leonhardt, C. Muratore, S.G. Walton, R.A. Meger, Surf. Coat. Technol. 188–189 (2004) 299.
bib0625 [124] P. Bodo, J.E. Sundgren, J. Vac. Sci. Technol. A 2 (1984) 1498.
bib0630 [125] P. Bodo, J.E. Sundgren, Thin Solid Films 136 (1986) 147.
bib0635 [126] J.W. Coburn, H.F. Winters, J. Appl. Phys. 50 (1979) 3189.
bib0640 [127] H.F. Winters, J.W. Coburn, Appl. Phys. Lett. 34(1) (1979) 70.
bib0645 [128] D.J. Ball, J. Appl. Phys. 143 (1972) 3047.
bib0650 [129] S.S. Lau, R.H. Mills, D.G. Muth, J. Vac. Sci. Technol. 9 (1972) 1196.
bib0655 [130] D.J. Stirling, Appl. Phys. Lett. 9 (1966) 326.


ISBN: 978-0-8155-2031-3; PII: B978-0-8155-2031-3.00002-8; Author:Martin; Document ID:00002; Chapter ID:c0010

bib0660 [131] P.W. Palmberg, C.T. Todd, T.N. Rhodin, J. Appl. Phys. 39 (1968) 4650.
bib0665 [132] M.R. Jordan, D.J. Stirland, Thin Solid Films 8 (1971) 221.
bib0670 [133] D.G. Lord, M. Prutton, Thin Solid Films 21 (1974) 341.
bib0675 [134] G. Shimaoka, J. Cryst. Growth 31 (1975) 92.
bib0680 [135] R.D. Ramsier, J.T. Yates Jr, Surf. Sci. Rep. 12 (1991) 243.
bib0685 [136] D. Menzel, R. Gomer, J. Chem. Phys. 41 (1964) 3311.
bib0690 [137] P.A. Redhead, Can. J. Phys. 42 (1964) 886.
bib0695 [138] M.L. Yu, Phys. Rev. B 19(12) (1979) 5995.
bib0700 [139] N. Inagaki, Plasma Surface Modification and Plasma Polymerization, Technomic Publishing Co., Lancaster, PA, 1996.
bib0705 [140] S. Thomas, J. Appl. Phys. 45 (1974) 161.
bib0710 [141] B. Carriere, B. Lang, Surf. Sci. 64 (1977) 209.
bib0715 [142] M.L. Knotek, V.O. Jones, V. Rehn, Phys. Rev. Lett. 43(4) (1979) 300.
bib0720 [143] D. Lichtman, Surf. Sci. 90 (1979) 579.
bib0725 [144] A.R. Burns, E.B. Stechel, D.R. Jennison (Eds.), Desorption Induced by Electronic Transitions, DIET-V, Springer, Berlin, 1992, and previous volumes.
bib0730 [145] K. Fukutani, Y. Murata, Surf. Sci. 390 (1997) 164.
bib0735 [146] S.G. Walton, B.L. Peko, R.L. Champion, Phys. Rev. B 58(23) (1998) 15430.
bib0740 [147] A. Hollander, R. Wilken, J. Behnisch, Surf. Coat. Technol. 116-119 (1999) 788.
bib0745 [148] I. Petrov, A. Myers, J.E. Greene, J.R. Abelson, J. Vac. Sci. Technol. A 12 (1994) 2846.
bib0750 [149] A.W. Benninghoven, F.G. Rudenauer, H.W. Werner, Secondary Ion Mass Spectrometry: Basic Concepts, Instrumentation Aspects, Applications, and Trends, Wiley, New York, 1987.
bib0755 [150] J.W. Coburn, E. Kay, Appl. Phys. Lett. 43 (1971) 435.
bib0760 [151] W.D. Sproul, D.J. Christie, D.C. Carter, Thin Solid Films 491 (2005) 1.

ISBN: 978-0-8155-2031-3; PII: B978-0-8155-2031-3.00002-8; Author:Martin; Document ID:00002; Chapter ID:c0010